A hybrid Pt/NbO/CNTs catalyst with high activity and durability for oxygen reduction reaction in PEMFC

A hybrid Pt/NbO/CNTs catalyst with high activity and durability for oxygen reduction reaction in PEMFC

Reza Alipour Moghadam Esfahani,*[a,b] Svetoslava K. Vankova,[b] E. Bradley Easton, [†a] Iraklii I. Ebralidze, [a] Stefania Specchia*[b]

[a] *University of Ontario Institute of Technology, Faculty of Science, Electrochemical Materials Lab, 2000 Simcoe Street North, Oshawa, Ontario L1H 7K4, Canada.*

[b] *Politecnico di Torino, Department of Applied Science and Technology, Corso Duca degli Abruzzi 24, 10129 Torino, Italy.*

Corresponding authors: reza.alipour@uoit.ca, stefania.specchia@polito.it

[†] Email: brad.easton@uoit.ca

Graphical Abstract

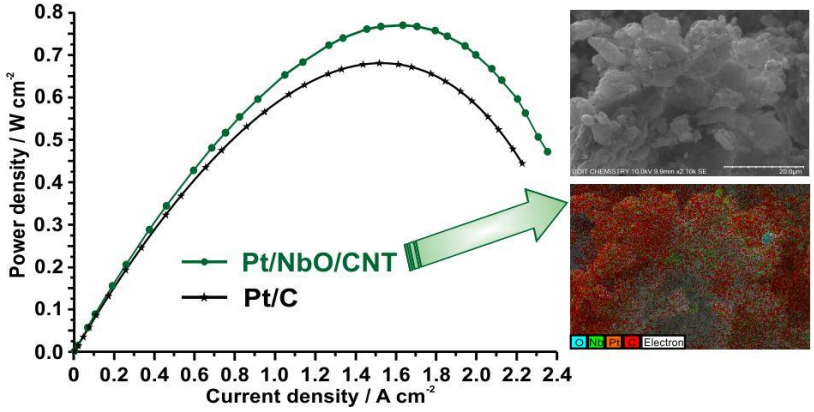

Highlights

- NbO suboxide support catalyst was prepared from Nb_2O_5.
- Pt/NbO/CNTs catalysts prepared from NbO suboxide and multi-wall carbon nanotubes.
- Excellent ORR activity & high durability after load cycling and startup/shout down stability test.
- Excellent activity in PEMFC with 772 mW cm^{-2} (Pt loading @ cathode: 0.15 mg cm^{-2}).
- Outstanding MEA stability with only 4% power loss.

Abstract

To improve the kinetics and durability of Pt-based electrodes toward the oxygen reduction reaction (ORR), high electroactive and stable catalysts were synthesized by depositing Pt over niobium oxide (NbO) supported on commercial multi-wall carbon nanotubes (CNTs). The Pt/NbO/CNTs, exhibits excellent electroactivity and stability toward ORR, reaching a high electroactivity of 57 mA mg_{Pt}^{-1}, higher than the Pt/CNTs and commercial Pt/C (20% Pt/C HiSPEC^{TM}). Moreover, the developed Pt/NbO/CNTs demonstrated outstanding durability under accelerated stress testing (AST) according to load cycling and startup/shutdown stability protocols. Proton exchange membrane fuel cells (PEMFC) tests with an MEA fabricated using Pt/NbO/CNTs showed excellent performance, with a low Pt loading down to 0.15 mg cm^{-2}, achieving a maximum power density of 772 mW cm^{-2}. Furthermore, a short-term durability test in PEMFC demonstrated only a 4% loss on the maximum power density at 80 °C. The superior electrocatalytic activity and durability of Pt/NbO/CNTs can be ascribed to the anchoring effect of Pt nanoparticles over the NbO/CNTs hybrid support, showing that the developed Pt/NbO/CNTs is a promising durable electrocatalyst for PEMFC applications.

Keywords: Proton exchange membrane fuel cells (PEMFC); Metal oxide support; Platinum electrocatalyst; Oxygen reduction reaction (ORR); Corrosion-resistance support; Stability and durability.

1. Introduction

Proton exchange membrane fuel cells (PEMFC) have attracted the consideration of many researchers as a highly efficient and clean energy source. Since one of principal drawback of electrocatalysts for oxygen reduction reaction (ORR) is their slow kinetics reaction, extensive studies on highly active and durable electrocatalysts have been performed, focusing to improve both ORR kinetics and durability [1-12]. Pt supported on carbon-based materials is one of the most common electrocatalysts for PEMFCs cathodic ORR [13]. However, the degradation of carbon supports and high Pt loading significantly hinder the wide adoption of PEMFC. The carbon corrosion, and the consequent loss of Pt nanoparticles (NPs), causes drastic reduction in electroactivity. This effect is particularly evident under harsh operating conditions of PEMFC, especially during prolonged open-circuit potential (OCP) or under repeated start up/shout down cycles [1,2,5,6]. To mitigate these problems, the use of metal oxides has been considered as an alternative method to promote an increased electroactivity and stability of Pt electrocatalyst. Metal oxides such as TiO_2, NbO_2, RuO_2, MoOx, exhibit high catalytic activity and strong interaction band with Pt [3,4,7–12,14]. Metal oxide supports provide a strong interfacial active band and enhance the catalytic activity towards ORR. Such an effect is attributed to the behavior of Pt electronic structure, which causes a decline in OH adsorption on Pt surface, through lateral repulsion from the OH or O on the oxide's surface [1]. This approach leads to decreasing the amount of noble metals required in the electrocatalyst, while increasing the electrocatalytic activity and durability. Moreover, by employing oxide metals as support materials, a more stable and homogeneous dispersion of Pt NP can be achieved [15–21].

NbO is a well-known reducible metal oxide, which shows high oxygen storage capacity with strong metallic interaction with Pt NP, displaying high conductivity, excellent catalytic stability, and corrosion resistance [1,12,22–28]. This study demonstrates the use of NbO, mixed with carbon nanotubes (CNTs), can promote electrocatalytic

activity and durability of Pt electrocatalyst. In fact, Pt/NbO/CNTs electrocatalysts exhibit higher electrocatalytic activity and stability compared to commercial Pt/C (HiSPEC™ 3000) electrocatalyst. Developing highly active and stable low Pt-based electrocatalyst for ORR will be the key action to enhancing PEMFC efficiency to deliver reliable, affordable, and environmental friendly energy.

2. Experimental

2.1 Chemicals

Commercial multiwall carbon nanotubes (CNTs: 6-9 nm × 5 μm 95 wt.%), chloroplatinic acid hexahydrate ($H_2PtCl_6{\cdot}6H_2O$, ≥37.50% Pt basis), sodium borohydride ($NaBH_4$, 98 wt.%), potassium hydroxide (KOH, 85% purity), sodium hydroxide (NaOH, 85% puririty), ethylene glycol (EG, 98 wt.%), polyvinylpyrrolidone (PVP, 98 wt.%), sulphuric acid 95-98 wt% (H_2SO_4), nitric acid (HNO_3, 70 wt.%), chloridric acid (HCl, 37 wt.%), Nafion® perfuorinated resin solution (5 wt.%), acetone (C_3H_6O, 99.5 wt.%), ethanol (C_2H_6O, 99.8 wt.%), 2-propanol (C_3H_8O, 99.5 wt.%), and Nafion® membrane NRE212 were purchased from Sigma-Aldrich. Niobic acid ($Nb_2O_5{\cdot}nH_2O$, type HY-340, water content ≈20 wt.%) was supplied by Companhia Brasileira de Metalurgia e Mineracão (CBMM, Brazil). A commercial 20 wt.% Pt/C (HiSPEC™ 3000, Johnson Matthey) was used for comparison test. All aqueous solutions were prepared using ultrapure deionized water (DW) obtained from a Millipore Milli-Q system with resistivity >18 mΩ cm^{-1}. Ultrapure N_2, O_2, and H_2 gasses were purchased by SIAD.

2.2 Synthesis of NbO

5 g $Nb_2O_5{\cdot}nH_2O$ was dispersed in 70 mL of 5 M NaOH aqueous solution under stirring for 2 h. Then, the prepared solution was transferred into a Teflon autoclave for a hydrothermal treatment at 120 °C for 50 h to obtain NbO_X. Subsequently, the treated NbO_x was washed with DW and 0.1 M HCl aqueous solution until the pH reached to values lower than 7. After that, the obtained NbO_x was filtered and dried in air at 100 °C for 2 h. The synthesized NbO_X was annealed at 950 °C (heating rate of 5 °C min^{-1}) for 4 h under a reducing atmosphere (H_2:N_2 10:90 vol.%) to obtain NbO.

2.3 Synthesis of hybrid support NbO/CNTs

100 mg CNTs was added to a solution of EG and ethanol (40:10 ml) and left stirring for 20 min. 1 wt.% PVP was added to the solution and left stirring for 2 h. The previously synthesized NbO was initially dispersed in EG, then added to the solution containing the CNTs and left stirring for 3 h. Then, the pH was reduced to 5 by adding HNO_3, and left stirring for 5 h. The obtained solution was filtered and washed with ultra-pure DW and left dry at 100 °C. The CNTs supported NbO (NbO/CNTs) was then annealed at 500 °C (heating rate of 10 °C min^{-1}) for 4 h under a reducing atmosphere H_2:N_2 10:90 vol.%.

2.4 Synthesis of Pt/NbO/CNTs

Pt/NbO/CNTs electrocatalysts were synthesized via the modified polyol method. NbO/CNTs was added to solutions of EG and ethanol (40:10 ml) and left stirring for 1 hr. Then, 1 wt.% PVP was added to the solution. 53 mg of

$H_2PtCl_6 \cdot 6\ H_2O$ (corresponding to 0.04 mmol of Pt) was dissolved into EG, added to each solution containing the NbO/CNTs and left stirring for 3 h at pH 11. The solution was heated to 120 °C under water-cooled reflux condenser for 5 hr. Then, temperature was reduced to 20 °C and solution was kept stirring for 5 h. The pH of the solution was brought to 4 by adding HNO_3 and left stirring for 12 h. The obtained solution was filtered, washed with DW, and the collected samples were dried at 100 °C. The obtained Pt/NbO/CNTs catalysts were annealed at 400 °C (heating rate of 5 °C min^{-1}) for 4 h under a reducing atmosphere (H_2:N_2 10:90 vol.%). For sake of comparison, a Pt/CNTs with same Pt amount was prepared.

2.5 Chemical-physical characterization of the electrocatalysts

The morphology of the synthesized electrocatalysts and the quantification of the metals content were observed by using a scanning electron microscopy (SEM) coupled with an energy dispersive X-ray (EDX) detector (Hitachi FlexSEM 1000). Transmission electron microscopy (TEM) was carried out using a Philips CM12 microscope. Thermogravimetric analysis (TGA) was performed using a TA Instruments Q600 SDT thermal analyzer. The Sample was heated from room temperature to 1000 °C at a rate of 10 °C min^{-1} under flowing air (20 mL min^{-1}), which enables the determination of the weight percent of the individual components. The phases and lattice parameters of the composite catalyst was characterized by using X-ray diffraction (XRD) employing Panalytical X'Pert PRO diffractometer with a PIXcel detector. The Cu Kα radiation, (λ= 0.15418 nm) operating at 40 kV and 30 mA used under the conditions of 2θ = 10–100° and 2θ step size = 0.03. The average crystallite size of the Pt particles was estimated using the Scherrer equation. The specific surface area of samples was determined by the Brunauer-Emmet-Teller (BET) method using a Quantachrome Nova 1200e BET analyzer within the relative pressure range of 0.1-0.9. Nitrogen adsorption isotherms were recorded at -196 °C within the relative pressure range of 0-1. Prior to adsorption, samples were placed in the cell and evacuated at 150 °C for 3 h under high vacuum. The surface composition of the NbO/CNTs and Pt/NbO/CNTs support and catalyst were studied by XPS, employing the Thermo Scientific K-Alpha Angle-Resolved system equipped with a monochromatic Al Kα (1486.7 eV) X-ray source and a 180º double focusing hemispherical analyzer with a 128-channel detector with effective charge compensation.

2.6 Electrochemical characterization of the electrocatalysts

The electrochemical evaluation of the Pt/NbO/CNTs, Pt/CNTs and Pt/C electrocatalysts were carried out in a three-compartment electrochemical cell using a multi-potentiostat (Bio-Logic SP150) and a rotating disk electrode instrument (RRDE-3A ALS Model 2323) or Pine Instruments. The electrochemical cell was equipped with a glassy carbon (GC) or gold disk working electrode (0.1256 cm^2), a graphite rod as a counter electrode, and a saturated calomel (SCE) as a reference electrode (each experiment repeated for three times). All potentials reported here were corrected to the RHE scale. The procedure for preparing the electrocatalyst ink and the RDE is reported in our previous study [29]. The Pt loading on the GC/gold electrode was 20 μg_{Pt} cm^{-2}, corresponding to 3 µL of the sonicated ink, micropipetted from the ink, deposited over working electrode and dried at room temperature. The Nafion® ionomer-to-catalyst ratio in the ink was equal to 0.1.

Cyclic voltammetry (CV) and electrochemical impedance spectroscopy (EIS) experiments were performed in N_2-saturated 0.5 M H_2SO_4 or 0.1M H_2SO_4 aqueous solution. CV were recorded varying the voltage in the range 0.05 to 1.25 V_{RHE}. Impedance spectra were collected over a frequency range of 100 kHz to 0.1 Hz at a DC bias potential of 0.425 V_{RHE} using Solartron 1470 multichannel potentiostat paired with a Solartron 1260 frequency response analyzer, controlled using Multistat software (Scribner Associates). ORR activity was assessed using linear sweep voltammetry (LSV) at rotating disk electrode in O_2-saturated 0.5 M H_2SO_4 aqueous solution. The electrochemical surface active area (ECSA, $m^2\ g^{-1}$) of the various electrocatalysts was determined from the Pt hydrogen desorption region between 0.06 V and 0.36 V_{RHE}, by integrating the total charge, normalizing with scan rate, Pt loading, and assuming a surface charge density of 210 μC cm_{Pt}^{-2} for a monolayer adsorption of hydrogen on Pt surface [2,30,31], according to the following formula:

$$ECSA = \frac{Q_H}{0.21\ .\ [Pt]}$$

CO stripping voltammetry (CO-SV) was performed in 0.5 M H_2SO_4 at a scan rate of 20 mV s^{-1} in the potential range of 0.05-1.25 V_{RHE}. Before the analysis, a flow-rate of CO was pre-adsorbed for 20 min while maintaining the working electrode at the constant potential of 0.06 V_{RHE}. Then, a flow rate of pure N_2 was introduced for 20 min to remove the excess CO dissolved in the solution before stripping the CO. The ex-situ electrochemical stability of the supports and catalysts were evaluated using ASTs that involved repeated cycling of the working electrode based on triangular-wave form at different potential range according to protocols developed by US Department of Energy. This potential ranges assures the accelerated corrosion of the support as well as the sintering of Pt NPs based on Pt oxide growth/removal, load cycling and start up/shout down fuel cells condition. The electrode health was monitored by periodic CV and EIS assessment throughout the AST. In addition, the ORR activity of each electrocatalysts was assessed before and after the AST.

2.7 PEMFC tests

The Pt/NbO/CNTs was used for a series of electrochemical tests in a Electrochem PEMFC station, and compared with Pt/C commercial. Nafion® 212 membranes were cleaned and fully protonated before use by first immersing them in 3% H_2O_2 at 80 °C for 1 h, then in 0.5 M H_2SO_4 at 80 °C for 2 h, and finally washing them in ultrapure DW for 2 h changing water every 30 min. The catalyst inks were prepared through dispersion of the electrocatalyst in a mixture of isopropanol and DW, and 32 wt.% Nafion® ionomer, and sonicating in ultrasonic bath for 30 min. The Pt loading was set at 0.15 $mg_{Pt}\ cm^{-2}$ for both for Pt/NbO/CNTs and Pt/C electrocatalysts. Both electrodes were prepared through spray deposition onto the gas diffusion electrodes (E-TEK ELAT), and then the electrodes dried at 70 °C. The MEA were assembled by hot-pressing the electrodes on the two sides of each membrane at 20 kg cm^{-2}, 50 bar, and 120 °C, for 90 sec.

PEMFC tests were performed by feeding pure fully humidified compressed hydrogen and oxygen, 120 and 200 NmL min^{-1}, respectively, at 1 bar backpressure. Before performing polarization curves, each membrane was conditioned with a series of 10 cycles running the cell at 0.6 V_{RHE} for 30 min and then at 0.4 V_{RHE} for another 30 min, and finally opening the circuit for 1 min, at a temperature of 70 °C [32]. Polarization curves were determined

at 30, 50, 70, and 80 °C. A durability tests were then performed on fresh MEA, maintaining it in operation at the maximum current density at 80 °C for 96 consecutive hours, repeating polarization curves every 24 h.

3. Results Discussion

3.1 Physical-chemical characterization of support and electrocatalysts

Figure 1 shows the XRD structural characterization of CNTs, Nb_2O_5, NbO, NbO/CNTs hybrid supports, and Pt/(NbO)/CNTs electrocatalysts. The starting CNTs has a large broad peak at 2θ = 26.1°, corresponding to graphite {002} reflection plane [33,34]. The starting Nb_2O_5 has typical peak orientations at 2θ = 26.3° {400}, 54.5° {622}, which its structure transferred to suboxide NbO after autoclave and heat treatment. The NbO/CNTs hybrid supports show the typical peaks corresponding to NbO, with characteristic reflections at 2θ = 36.2° {111}, 42.2° {200}, 60.9° {220}, 73.1° {311}. The Pt/NbO/CNTs catalysts have peaks orientation at 2θ = 40.32° {111}, 46.75° {200}, 68.1° {220}, 81.8° {311}, and 86.1° {222}, which are indexed to the face-centered cubic structure of Pt crystallites present on NbO/CNTs hybrid supports. Compared to the standard card of Pt (ICDD card 01-087-0640), all corresponding Pt peaks were shifted toward higher angles, indicating a diminution of lattice spacing. This phenomenon can be attributed to the strong metallic support interaction (SMSI) between Pt NPs and NbO/CNTs hybrid support [35]. Moreover, the peak at 2θ = 40.32° is broad and intense, sign that Pt NPs are essentially orientated towards the Pt {111} plane, that is the most stable and highly active toward ORR. In fact, this plane contains hexagonally packed Pt atoms and does not undergo surface reconstruction, unlike Pt {100} and Pt {110} surfaces [2,35,36]. The Pt crystallite sizes were calculated from the widths of the {220} peaks using the Scherrer-Debye equation. The mean crystallite size of Pt particles obtained was in the range of 2-4 nm, which is in good agreement with TEM results.

Figure 2 shows the TEM and overall SEM image obtained for Pt/NbO/CNTs catalyst at different magnifications. The Pt NPs are well dispersed over the NbO/CNTs support (**Fig 2a**), where the TEM (HRTEM) image showed Pt NPs were dominated by octahedron {111}-*d*-spacing of ~ 0.223 nm in agreement with XRD result (**Fig. 2b-2c**) [37–39]. **Figure 2c** demonstrate the lattice fringe of NbO nanoparticles. The fringe spacing is calculated to be ~0.375 nm ±0.01 nm, corresponding to the {001} lattice spacing. Compare to Nb_2O_5 with *d*-spacing of 0.39 nm ±0.01 nm, the NbO exhibited reduced *d*-band due to oxygen vacancy in its lattice structure [40–42]. **Figure (2d-2f)** shows overall SEM image of Pt/NbO/CNTs catalyst with the relative EDS elemental distribution map. Figure 2f shows Pt nanoparticles are finely distributed over NbO/CNTs hybrid support with no sign of agglomeration or cluster formation.

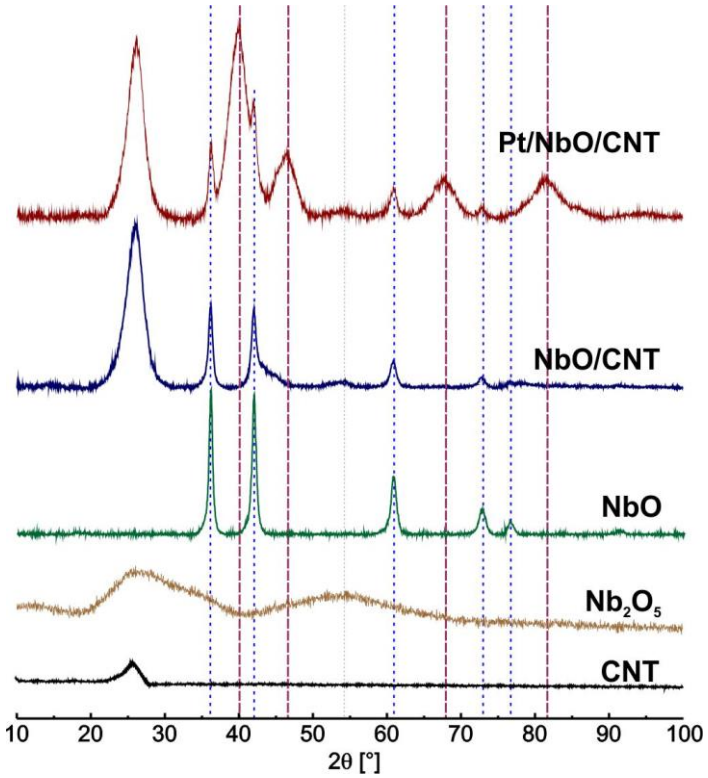

Figure 1. XRD pattern of CNTs, Nb_2O_5, NbO, Nb/CNTs, and Pt/NbO/CNTs electrocatalysts.

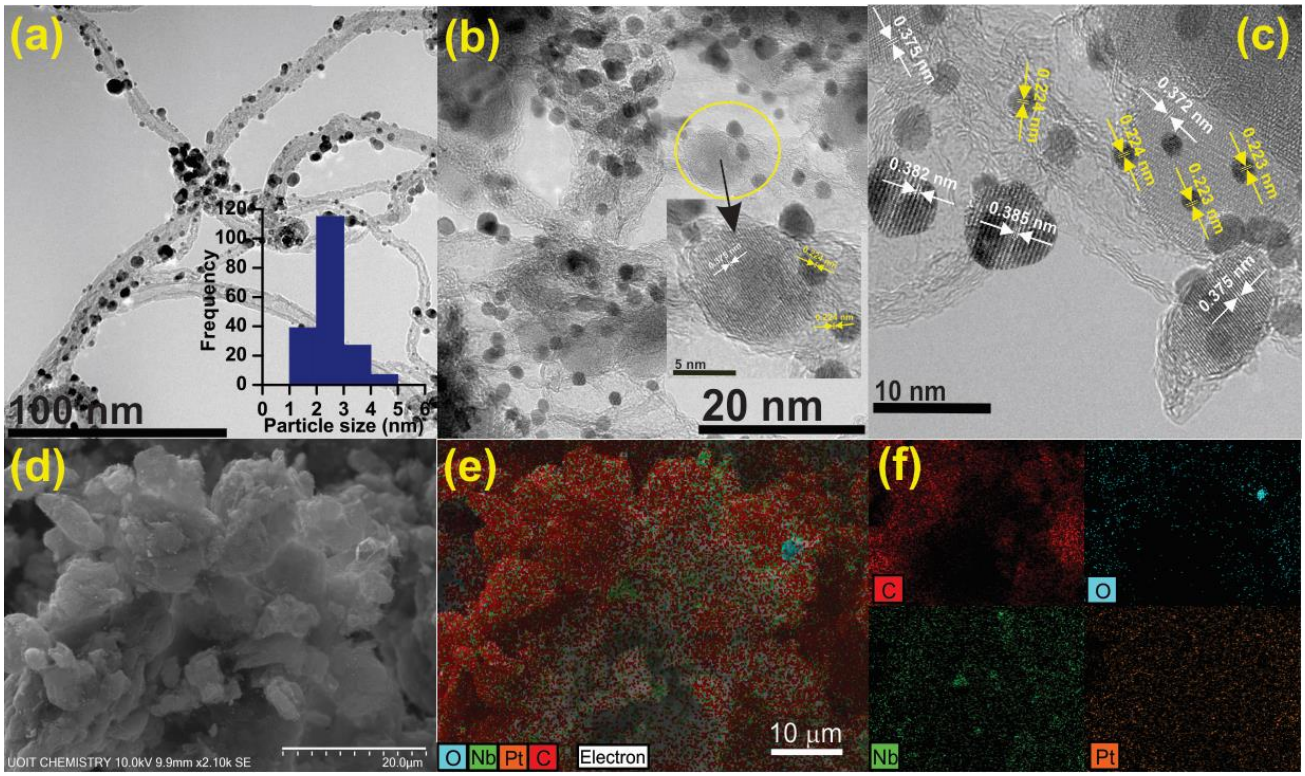

Figure 2. (a, b and c) TEM image corresponding to Pt/NbO/CNTs, (d, e and f) SEM-EDX elemental mapping obtained for Pt/NbO/CNTs electrocatalyst.

The electronic interaction between Pt and the NbO/CNTs hybrid support were investigated by using XPS spectra and the results are shown in (**Fig. 3**). The Nb double peaks of $3d_{5/2}$ and $3d_{3/2}$ levels with splitting-value of Δ= 2.78 eV were located at binding energies of 207.42 eV and 210.2 eV, respectively [43,44]. Compare to pure Nb_2O_5 with

Nb double peaks of $3d_{5/2}$ and $3d_{3/2}$ levels at 207.1 eV and 209.88 eV binding energies, the reduced NbO oxide exhibited binding energies of 207.42 eV and 210.2 eV. In fact, 0.32 eV shift to higher binding energy in the Nb 3d levels compared to defect-free Nb_2O_5 is caused by surface oxygen vacancy defects in the NbO support (**Fig. 3a**). Furthermore, it was found out for Pt/NbO/CNTs, the NbO peaks were shifted to higher binding energy by 0.18 eV compared to Nb of NbO/CNTs (0.5 eV compared to pure Nb_2O_5) (**Fig. 3b**). Such this shift to higher binding energy could be due to Pt-NbO metallic binding. The Pt analysis shows doublet peaks in the 4f region referring to $4f_{7/2}$ and $4f_{5/2}$, where the deconvolution of the Pt spectrum reveals two pairs of separate doublet peaks in each region. The high intensity doublet peaks with splitting-value of Δ= 3.35 eV attributed to metallic Pt (Pt^0), located at the binding energies of 71.7 eV and 75.05 eV, respectively [12,45,46]. The peak at binding energy of 71.7 eV, referring to Pt^0 $4f_{7/2}$ reveals 0.7 eV positive shift towards higher binding energy compared to the $4f_{7/2}$ conventional value of Pt/C. This shift to higher binding energy corresponds to induced positive charge on the dispersed Pt NPs due to the interaction between Pt NPs and NbO support through SMSI effect which positively influenced the d-band state of Pt NPs [47–49]. Moreover, the low-intensity doublet peaks at binding energies of 73.42 eV and 76.76 eV assigned to Pt^{2+} species due to surface oxide/hydroxide (**Fig. 3c**).

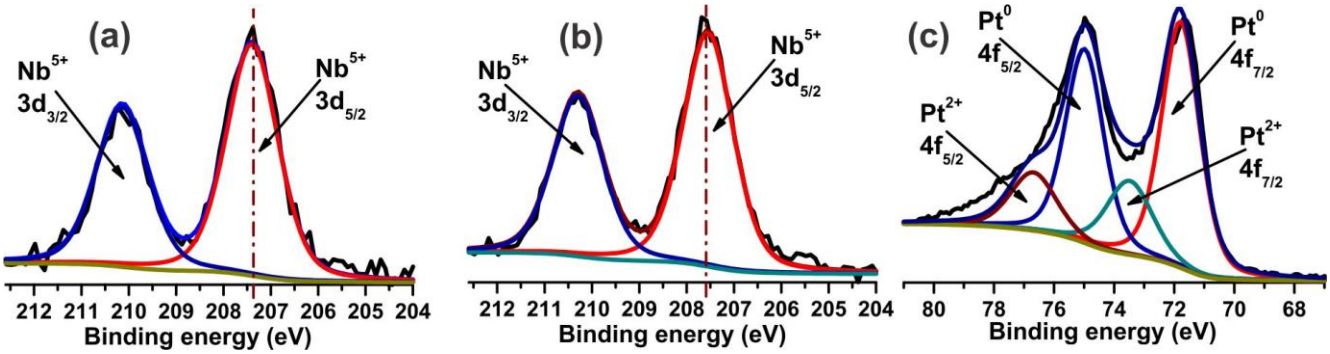

Figure 3. XPS spectra of the (a) NbO/CNTs support, (b) and (c) Pt/NbO/CNTs catalyst.

Figure 4 shows the TGA and DTG curves obtained under flowing air for CNTs, NbO/CNTs, and Pt/NbO/CNTs samples. All samples showed moisture and volatile matter loss in temperature range of 80-250 °C. The CNTs underwent carbon combustion in two step, the main weight loss occurs in temperature range of 450-600 °C due to the oxidation of un-filled CNTs [50,51]. The second weight loss of CNTs that occurs at slight higher temperature is referred to the oxidation of polyaromatic carbon shells present in the CNTs, due to ethanol as a carbon source [52,53]. The NbO/CNTs exhibited carbon combustion between 500-650 °C due to the presence of NbO, which shield the CNTs. On other hand, the Pt/NbO/CNTs shows carbon combustion in a lower temperature range, between 420-520 °C, due to presence of Pt catalyst, which facilitates the combustion reaction. The residual weight percentage of samples at 800 °C was used to calculate the weight percentage of NbO and Pt content. Moreover, the TGA and DTG analysis of samples under inert atmosphere (Argon) are presented in (**Fig. S1**).

The surface areas and porous characteristics of CNTs and NbO/CNTs support were investigated by nitrogen ad/desorption measurements. The BET isotherms and BJH pore size distribution curves of both support are shown in (**Fig. 4c**). Both of CNTs and NbO/CNTs supports show typical type IV isotherms indicating the presence of mesoporous structure. Upon deposition of the NbO, the surface area of CNTs slightly reduced from 364.1 $m^2 g^{-1}$ to

331.1 m^2 g^{-1} due to NbO particles which physically block access to some of the CNTs pores [54]. The changes in BET surface area, pore volume and size of CNTs after NbO deposition reported in **Table1**. The pore size distribution plots from the nitrogen adsorption isotherm of the CNTs and NbO/CNTs were presented in the inset of (**Fig. 4c**). Both support presented pore size distribution peak approximately in range of 2 nm to 15 nm with an average diameter of 4-6 nm, which indicate the CNTs and NbO/CNTs exhibited mesoporous structure with high surface, suitable support for Pt electrocatalyst.

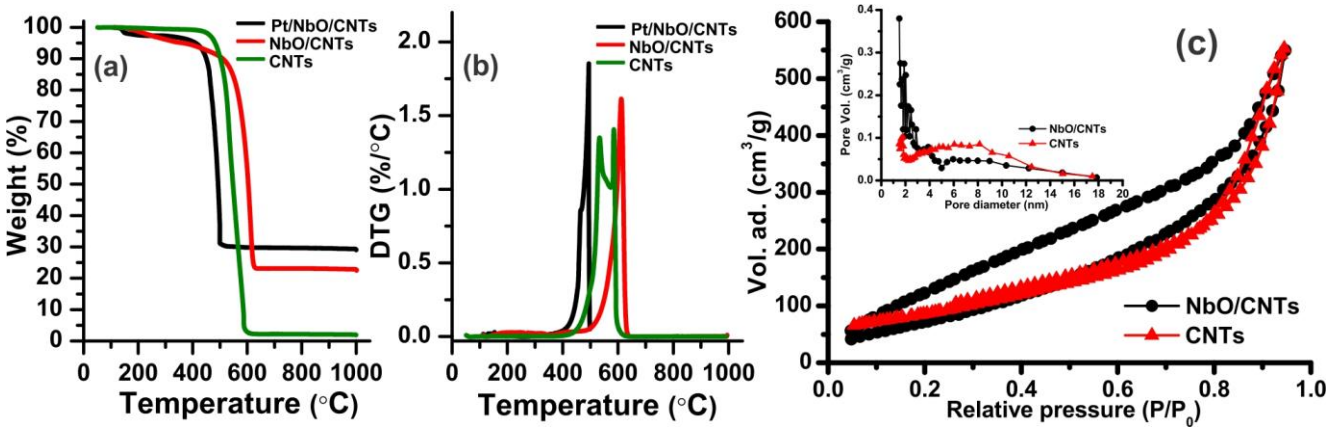

Figure 4. Air-thermo analysis of CNTs, NbO/CNTs, and Pt/NbO/CNTs; (a) TGA, (b) DTG, (c) BET surface area analysis via nitrogen ad/desorption isotherms and corresponding pore size distribution (inset) of CNTs, NbO/CNTs.

Table 1. BET analysis of supports

Sample	BET surface area [m^2 g^{-1}]	Pore volume [cm^3 g^{-1}]	Pore size [nm]
NbO/CNTs	331.1	0.754	1.56
CNTs	364.1	0.885	1.98

3.2 NbO support electroactivity and stability

Figure 5 shows the electrochemical activity of NbO support. The CV of NbO exhibited small reversible redox peaks, typical for pseudo-capacitive materials. The CV results reveal that NbO does not contribute during hydrogen ad/desorption regime, and no specific oxidation or reduction current peak observed, a sign of NbO high stability in acid medium [55]. The AST results on NbO up to 5,000 cycles indicates that NbO is perfectly stable in 0.5 M H_2SO_4 aqueous electrolyte over the entire range of applied potential (**Fig. 5a**). The ORR activity of NbO support was assessed before the AST (**Fig. 5b**). The NbO exhibits limited activity, with onset potential of 0.7 V_{RHE} for O_2 reduction followed by high half-wave potential of 0.2 V_{RHE}. **Figure 5c-5d** displays the EIS response of the NbO support over the course of the AST; data is shown as Nyquist and capacitance plots. During a stability test, the key parameters to monitor is the length of Warburg region in order to determine any changes in R_Σ ($R_\Sigma = R_{electronic} + R_{ionic}$) and C_{dl} (low frequency limiting capacitance) which is indicative of any changes in the interfacial surface area of the electrode. The Nyquist plot of NbO support exhibited short Warburg regions assign to its high electronic and ionic conductivity. The Warburg length slightly decreased over the course of the stability test due to enhance accessibility of catalyst surface layer to electrolyte solution and consequently enhancing the total conductivity of

catalyst layer [46,56]. The limiting capacitance of NbO shows visually no change over the course of 5,000 cycles, assign to highly stable catalyst surface layer (**Fig 5e-5f**).

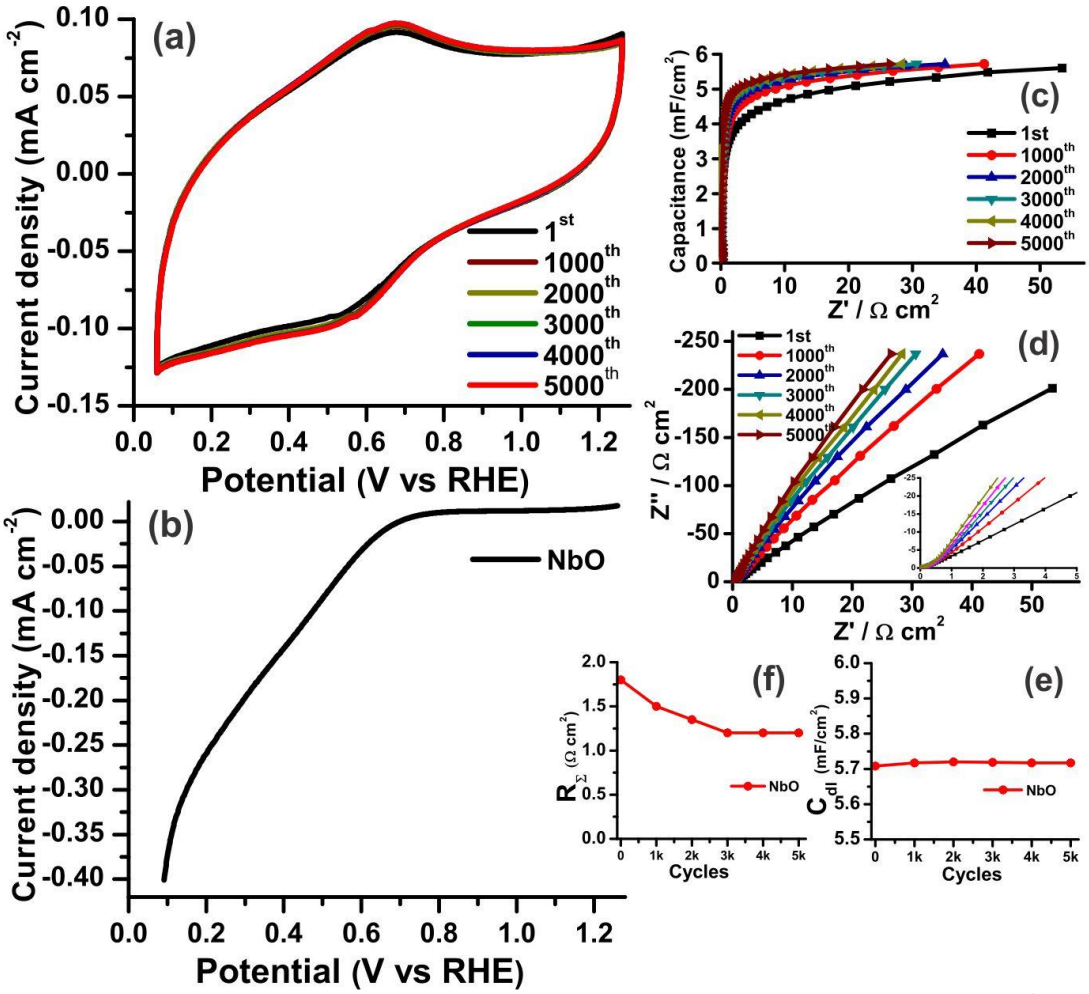

Figure 5. (a) CV recorded in 0.5 M H_2SO_4 N_2-saturated solution, scan rate of 50 mV s^{-1} at 25 °C, (b) LSV recorded in 0.5 M H_2SO_4 O_2-saturated solution, 900 rpm, scan rate of 5 mV s^{-1} at 25 °C, (c) Capacitance plot, (d) Nyquist plot, (e, f) R_Σ and C_{lim} of electrocatalysts obtained at DC bias potential of 0.425 V_{RHE}.

3.3 Electroactivity of electrocatalysts

Figure 6a shows the CVs of electrocatalysts. All electrocatalysts exhibited two anodic and two cathodic peaks with well reversibility in hydrogen region that can be assigned to uniform dispersed polycrystalline Pt particles over the surface of the supports. For all electrocatalysts, the CVs exhibit the three characteristic regions: the hydrogen ad/desorption peaks appear at a potential range between 0.06–0.36 V_{RHE}, the double layer capacitance, and the region of Pt oxide formation with the reduction in the higher potential [22,55,57–60]. The Pt/NbO/CNTs electrocatalyst exhibited earlier Pt reduction cathodic peak at 0.76 V_{RHE} compare to other catalysts, and highest ECSA value of 81.62 m^2 g^{-1} compare to Pt/CNTs and Pt/C with ECSA value of 76.85 and 73.66 m^2 g^{-1}, respectively (**Table 2**). The presence of NbO on hybrid support plays a favorable role, which attributed to uniform dispersion of Pt NPs over the NbO/CNTs hybrid support and faster polishing the Pt surface from formed oxide [14,22–25].

Figure 6b compares the ORR activity of electrocatalysts. All electrocatalysts exhibited diffusion-controlled regime at a potential less than 0.6 V_{RHE}, reaching limiting current densities between 5–5.5 mA cm^{-2}. The region of mixed diffusion kinetic control is in potential range of 0.6–0.9 V_{RHE}, and kinetic region is in potential higher than 0.9 V_{RHE}. The Pt/NbO/CNTs shows high ORR electroactivity with onset potential of 1.0 V_{RHE} for O_2 reduction as well as high half-wave potential of 0.86 V_{RHE} compared to a halfwave potential of 0.83 and 0.81 V_{RHE} for Pt/CNTs and commercial Pt/C, respectively. The Pt/NbO/CNTs achieved outstanding ORR activity, producing 1.14 mA cm^{-2} at 0.9 V_{RHE} compared to only 0.86 and 0.57 mA cm^{-2} for Pt/CNTs and commercial Pt/C. In general, the ORR initiates by O_2 molecular adsorption on the surface of Pt electrocatalyst. The Pt-O_2 either hydrogenated to Pt-OOH ($O_2 + H^+ + e^- \rightarrow$ OOH), which later dissociates into adsorbed O and OH, or undergoes direct splitting of the O–O bond in the presence of oxygen vacancy sites on the NbO support that resulted to hydrogenation of O or OH to H_2O [14,61,62]. Surface defects on NbO, especially oxygen vacancies, have been considered as active sites for water splitting. In fact, employing NbO support has the undoubted advantages of reducing the OH adsorption on Pt surface and preventing the dissolution of Pt from the surface of the support [1,7]. Also, the enhancement in ORR activity of Pt/NbO/CNTs could be correlated with reduction of the Pt d-bond length, due to the SMSI between NbO support and Pt NPs that weakens the interaction between Pt and the adsorbed oxygenated species and leads to higher electroactivity compared to that Pt/CNTs and commercial Pt/C catalysts [21,49,63,64]. Tafel Plots using mass-transfer-corrected kinetics are shown in (inset of **Fig. 6b**). The electrocatalysts display similar trends, indicating that the order of reaction should be the almost the same, while Pt/NbO/CNTs exhibited faster kinetics reaction at high potential compare to Pt/CNTs and Pt/C. The Tafel plot shows double slop region, lower Tafel slope at high potentials (–59.2 mV/dec) compared to that at low potentials (–118.4 mV/dec) due to site-blocking effect by OH or O at high potentials cause the Tafel slope to deviate from its intrinsic value at low potentials [65,66]. Moreover, to understand the influence of NbO support on electron-transfer kinetics involved in the ORR, and determine the mechanism of reaction, (whether O_2 is reduced directly to water via a direct 4 electrons or an indirect two-step 2+2 electrons), polarization curves of ORR were measured at various rotation speed (**Fig. S2**). Both Pt/NbO/CNTs and Pt/CNTs electrocatalysts exhibited an enlarged current intensity by increasing the rotation speed, due to the enhancement of O_2 diffusion to catalyst layer [49]. The Koutecky-Levich plot shows linear trend with a parallel slope at different potentials for both catalysts, enabling the calculation of the number of electrons, equal to 4.18 and 3.9 for Pt/NbO/CNTs and Pt/CNTs, respectively (**Fig. S2**).

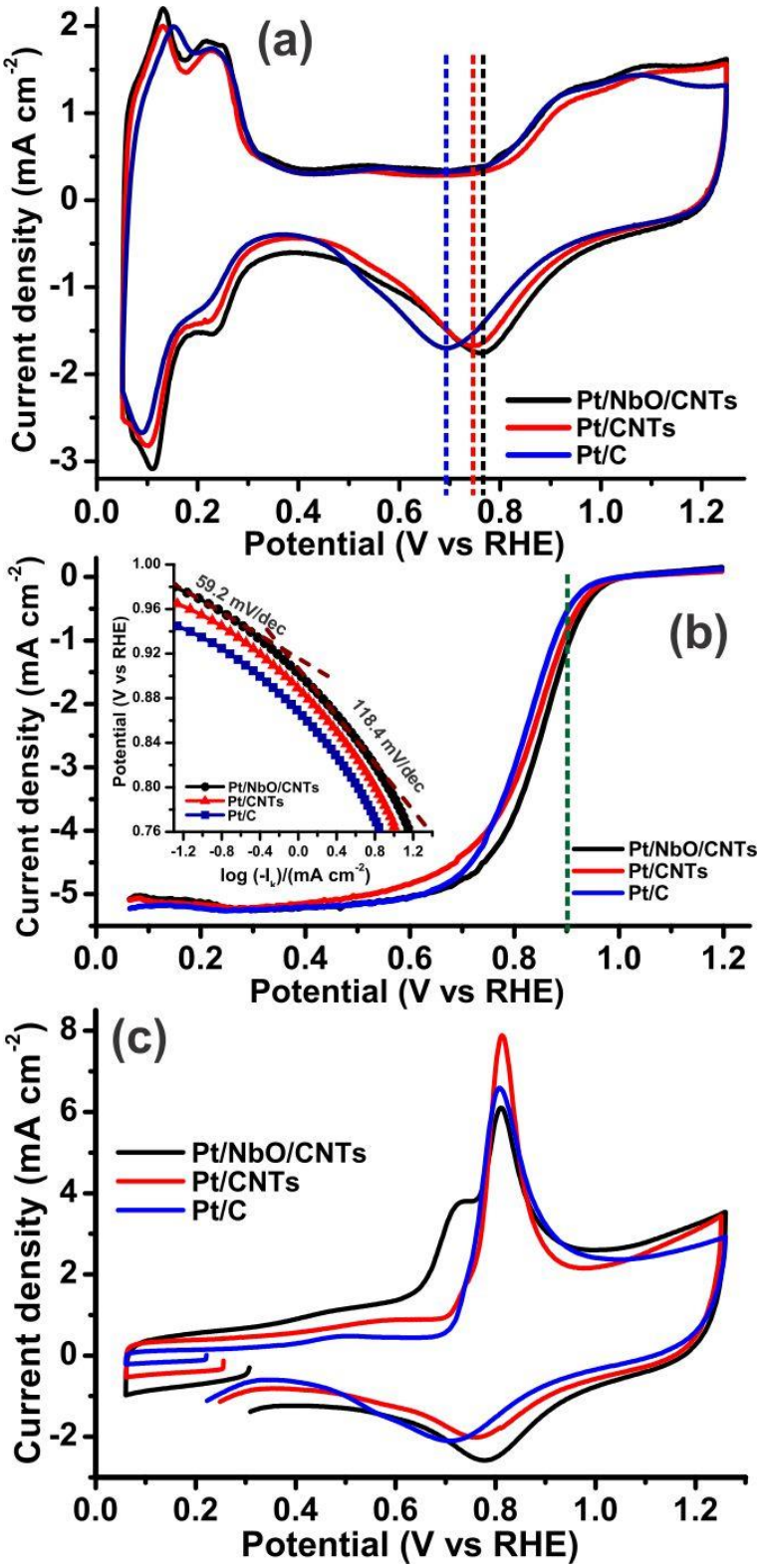

Figure 6. Electroactivity of catalysts; (a) CV recorded in 0.5 M H_2SO_4 N_2-saturated, scan rate of 50 mV s^{-1}; (b) LSV recorded in 0.5 M H_2SO_4 O_2-saturated, 900 rpm, scan rate of 5 mV s^{-1}; (c) CV of CO oxidation recorded in 0.5 M H_2SO_4, scan rate of 20 mV s^{-1}.

Figure 6c shows CO stripping voltammograms obtained for electrocatalysts. The Pt/NbO/CNTs shows an enhancement in CO oxidation activity, attributed to a faster removal of CO species. The Pt/NbO/CNTs displays a

double shoulder peak of CO oxidation, due to NbO support and Pt crystals orientation in structure of electrocatalyst, which weakens bonding with CO [67]. The Pt/NbO/CNTs displays the earlier onset potential of 0.3 V_{RHE} corresponding to CO oxidation with an evident pre-shoulder at potential of 0.6 V_{RHE}, achieving to maximum current at 0.8 V_{RHE}. On the other hand, both Pt/CNTs and Pt/C catalysts present onset and maximum current of CO oxidation at potential of 0.71 and 0.8 V_{RHE}, respectively. In addition, The Pt/NbO/CNTs exhibited the cathodic Pt reduction peak at earlier potential of 0.79 V_{RHE}, compared to Pt/C and Pt/CNTs. Employing NbO as a support has the advantages of weakening the CO adsorption on Pt surface by lateral repulsion from the OH or O on the suboxide's support surface and stripping the CO from the Pt surface in lower potential. In fact, water dissociation over the metals oxide support starts at lower potential to provide OH species at the interface Pt-NbO, which results to reducing the anodic overpotential, while CO species are going to be oxidized to CO_2 over the Pt-NbO interface. Moreover, availability of NbO oxygen vacancy on the surface helps to oxidize the adsorbed CO on Pt surface faster, and the oxides surface is replenished through a redox reaction with water [28,68–70]. **Table 2** summarizes the key parameters of the electrocatalysts characterization;

$$NbO + H_2O \rightarrow NbO \cdots OH_{ads} + H^+ + e^-$$

$$Pt \cdots CO_{ads} + NbO \cdots OH_{ads} \rightarrow Pt + NbO + CO_2 + H^+ + e^-$$

Table 2. Electrochemical characterization of electrocatalysts

Catalyst	NbO [wt.%]	Pt [mg cm^{-2}]	$ECSA_{H2}$* [m^2 g^{-1}]	$ECSA_{CO}$** [m^2 g^{-1}]	I @ 0.9 V [mA cm^{-2}]	Mass activity [mA mg^{-1}]
Pt/NbO/CNTs	19	0.02	81.62	88.43	1.14	57
Pt/CNTs	-	0.02	76.85	83.27	0.86	43
Pt/C	-	0.02	73.66	82.56	0.57	28.5

*The ECSA was determined by integrating the charge associated with H-UPD (210 mC cm_{Pt}^{-2})

**The ECSA was determined by integrating the charge associated with CO-UPD (420 mC cm_{Pt}^{-2})

3.4 Durability of electrocatalysts

Protocol (I): Cycling through Pt oxide growth/removal

In addition to high electrocatalytic activity, stability and durability are important factors for electrocatalysts in order to be considered for PEMFC application. The ex-situ stability test was performed on all catalysts using AST protocol, which subjects each catalyst to triangular-wave form potential cycling in the range of 0.05-1.25 V_{RHE} in 0.5 M H_2SO_4 at 25 °C. Under this protocol the stability of Pt NPs against agglomeration/dissolution over the support was evaluated. We have found that this protocol exacerbates Pt NPs size growth since it cycles through Pt oxide growth/stripping without causing corrosion on most carbon supports [46,48,56]. **Figure 7a** shows the AST results on Pt/NbO/CNTs electrocatalyst for 5000 potential cycles performed with scan rate 100 mV s^{-1}. The Pt/NbO/CNTs catalyst shows an interesting stability and durability performance compare to Pt/CNTs and Pt/C catalysts (**Fig. 7a, 7b and S2**). The Pt/NbO/CNTs shows virtually no changes over the course of stability with only 5% loss of its ECSA, while Pt/CNTs and Pt/C presented 64.4% and 73.2% loss of ECSA, respectively (**Fig 7c**). To further investigate on stability of electrocatalysts, the EIS tests were performed, since it can provide information about changes in conductivity and resistance in the catalyst layer under different conditions, as well as insight into degradation mechanisms [71–73]. **Figure 7d-7e** show the R_Σ and C_{dl} variation of electrocatalysts over the course of

stability. The Pt/NbO/CNTs shows short Warburg length assign to high electronic conductivity of NbO/CNTs support and R_Σ follow stable trend during stability means no change in ionic and electronic conductivity of support. Both Pt/CNTs and Pt/C catalysts show decreasing in R_Σ during AST due to enhanced catalyst layer hydration. The Pt/NbO/CNTs exhibited almost no change in C_{dl} owing to excellent stability of the catalyst surface layer and Pt NPs, while Pt/CNTs and Pt/C exhibited decreasing in C_{dl}, characteristic response of Pt NPs agglomeration/dissolution in absence of support corrosion [74,75]. The ORR activity of catalysts was assessed before and after the AST (**Fig. 7f**). The Pt/NbO/CNTs exhibits outstanding activity, with a high onset potential of $1V_{RHE}$ for O_2 reduction followed by high half-wave potential ($E_{1/2}$) of 0.86 V_{RHE} compared to a half-wave potential of 0.83 and 0.81 V_{RHE} for the Pt/CNTs and commercial Pt/C (**Fig. S3**). Pt/NbO/CNTs illustrated excellent durability by only loss 12.6% of its initial mass activity at 0.9 V_{RHE} by shifting to lower potential, while Pt/CNTs and Pt/C exhibited massive degradation, losing 52% and 75% of their initial ORR activity at 0.9 V_{RHE} respectively. (CV, EIS and ORR plots for this AST can be found in **Fig. S3**).

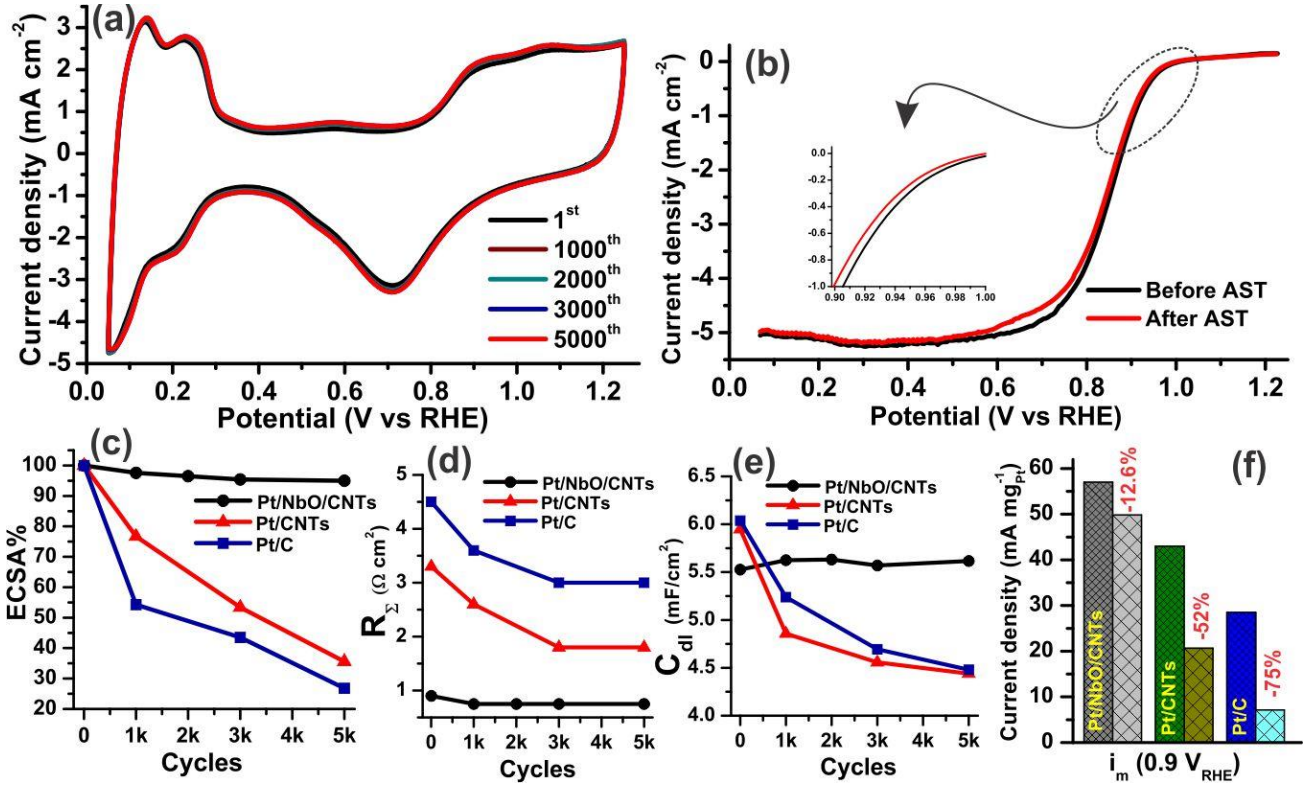

Figure 7. (a) Variation in the CV response of the Pt/NbO/CNTs, (b) ORR activity of Pt/NbO/CNTs before and after AST, (c) ECSA variation of the electrocatalysts over the course of AST (protocol I), (d, e) R_Σ and C_{lim} of electrocatalysts obtained at DC bias potential of 0.425 V_{RHE}, (f) ORR mass activity (i_m) of electrocatalysts.

Protocol (II): Ex-situ Load Cycling

The ex-situ stability of electrocatalysts were evaluated according to fuel cell load cycling via triangular-wave potential cycling in the range of 0.6-1 V_{RHE} for 30,000 cycles in 0.5 M H_2SO_4 at 25 °C. This US Department of Energy (DoE) based protocol is commonly used to evaluate the stability of Pt NPs against dissolution/agglomeration [76–79]. In fact, this stability test shows the significance of SMSI effect on stabilization of Pt NPs over the

supporting materials under fuel cell relevant conditions that avoids support corrosion. The change in key electrochemical parameters over the course of this AST for each catalyst is shown in **Figure 8**. Pt/NbO/CNTs exhibited excellent stability by showing only a 7.4% decay in ECSA, with no change in CV shape. This indicates a strong interaction between Pt NPs and NbO/CNTs support (**Fig. S3**). The Pt/CNTs and commercial Pt/C show 18.3% and 47.6% decay in ECSA, which indicated Pt NPs are more stable on CNTs support [80,81]. The EIS responses for all catalysts showed that the R_{Σ} decreased over the initial 5000 cycles of AST due to enhanced catalyst layer hydration (**Fig. 8b**). On the other hand, C_{dl} of both Pt/NbO/CNTs and Pt/CNTs catalysts after slight increase at beginning, remained almost unchanged over the course of AST (**Fig. 8c**), while the Pt/C illustrated 12% decrease on C_{dl} over the course of AST, which is characteristic of Pt NPs dissolution/agglomeration being the dominant degradation mechanism of catalyst [73]. The ORR activity of all catalysts was assessed before and after the AST (**Fig. 8d**). The Pt/NbO/CNTs and Pt/CNTs electrocatalysts showed ORR activity (i_m) decline of 7%, and 23.4% of their initial after 30K cycling under AST, respectively, while Pt/C loss 41.2% of its ORR activity. The Pt/NbO/CNTs exhibited only 5.5 mV decrease in $E_{1/2}$, while 15 and 40 mV decay in $E_{1/2}$ was observed for Pt/CNTs and Pt/C electrocatalysts, respectively. According to US DoE targets, electrocatalysts should not loss more than 40% of their initial activity after stability testing under load cycling protocol (0.6-1 V_{RHE}), which in this regard both Pt/NbO/CNTs and Pt/CNTs could meet the DoE target. (CV, EIS and ORR plots for this test can be found in **Fig. S4**).

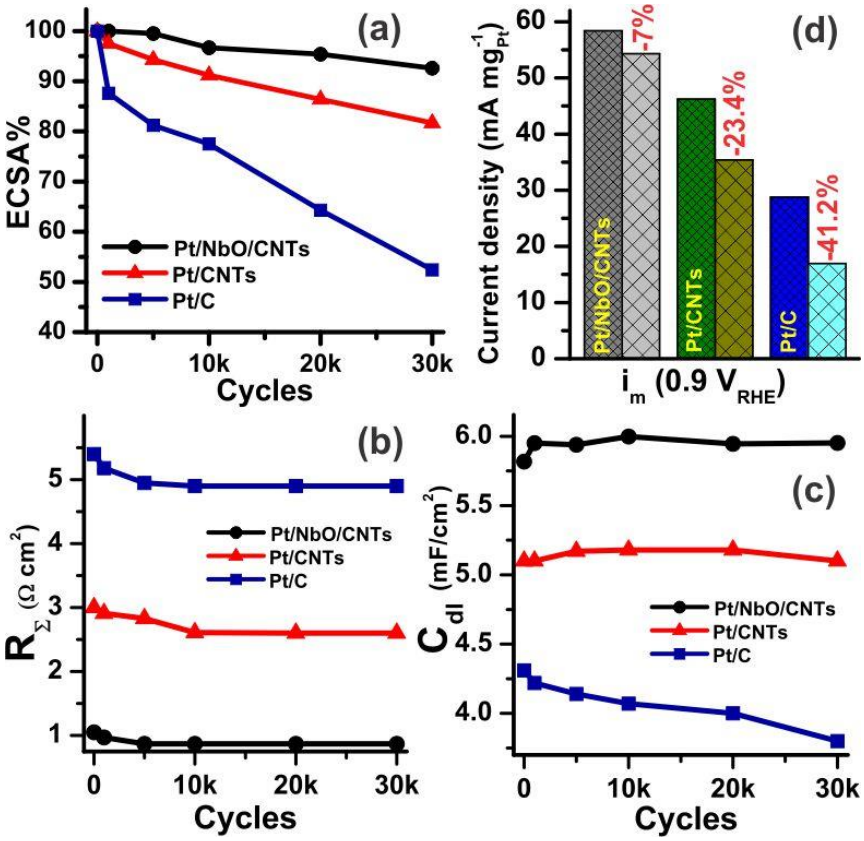

Figure 8. (a) ECSA variation of the electrocatalysts over the course of AST (protocol II), (b, c) R_{Σ} and C_{lim} of electrocatalysts obtained at DC bias potential of 0.425 V_{RHE}, (d) ORR mass activity (i_m) of electrocatalysts.

Protocol (III): Ex-situ Startup/Shutdown

The *ex-situ* stability of electrocatalysts was evaluated according to fuel cell vehicle startup-shutdown condition, using a potential triangular-wave form between 1-1.5 V_{RHE} at a scan rate of 500 mV/s in 0.1 M H_2SO_4 for 10,000 cycles. By employing this protocol, the stability of NbO/CNTs, and carbon supports against corrosion and stability of Pt NPs over the supports against dissolution/agglomeration were assessed [82]. Over the course of stability test no sign of degradation was observe on double layer region of Pt/NbO/CNTs catalyst. The ECSA was remained quite stable, showing only 11.4% decay comparable with Pt/CNTs and Pt/C, which loss 32.2% and 78.5% of their initial ECSA, respectively (**Fig. 9a**). The EIS response of Pt/NbO/CNTs was virtually unchanged, with constant trend of R_Σ and C_{dl} throughout the AST (**Fig. 9b-9c**). on the other hands, for both Pt/CNTs and Pt/C, the R_Σ increased steadily throughout the AST and C_{dl} initially increased during initial 3000 cycles, due to the oxidative formation of pseudo-capacitive groups on the carbon surface [77]. C_{dl} declined upon continued cycling for both electrocatalyst but more intensely for Pt/C. This EIS response on C_{dl} (initially increasing and then decreasing) follow by increasing in R_Σ, is characteristic of carbon support corrosion [73]. **Figure 9d** compares the ORR activity (i_m) of all catalysts before and after the AST. Pt/NbO/CNTs showed high durability by only a 7 mV and 17.1% decay in $E_{1/2}$ and ORR mass activity after 10,000 cycles, respectively. On the other hand, Pt/CNTs and Pt/C show 24 mV and 106 mV decay in $E_{1/2}$, respectively, follow by loss of 40.45% and 93% of their initial activity, due to Pt NPs sintering and carbon corrosion. According to DoE statement, electrocatalysts shouldn't loss more than 40% of their initial activity under startup-shutdown (1 - 1.5 V_{RHE}) stability test. In this regard, Pt/NbO/CNTs showed high stability and durability, which makes it suitable electrocatalyst for ORR. (CV, EIS and ORR plots for this AST can be found in **Fig. S5**). Also listed in **Table 3** are the reported electroactivity and stability of several other catalysts that employ metal oxide-based supports.

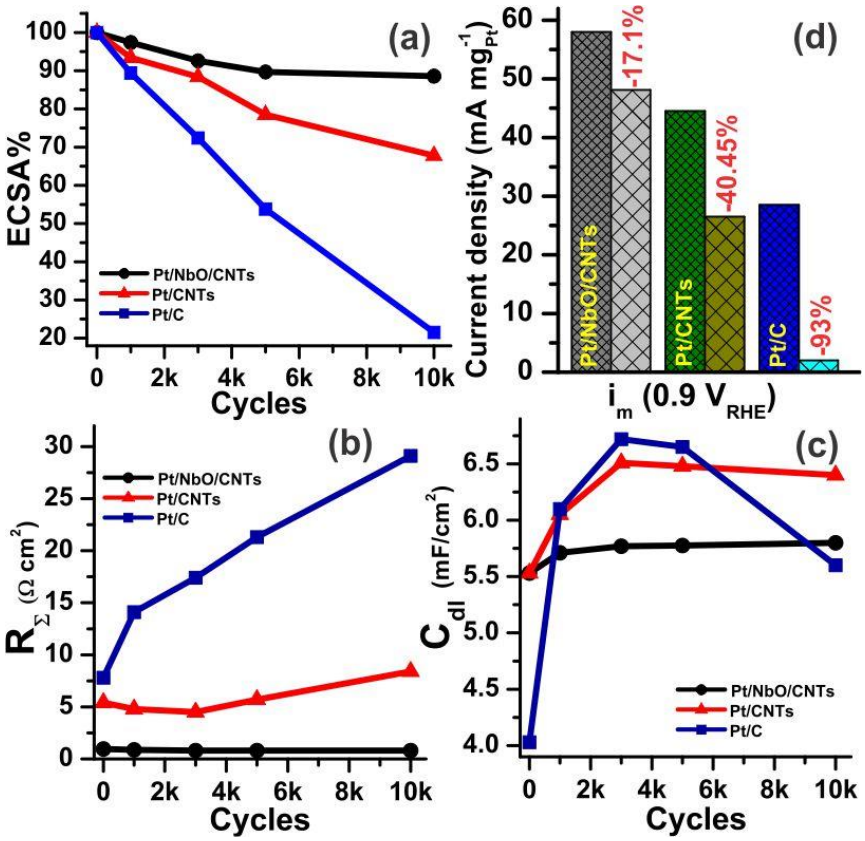

Figure 9. (a) ECSA variation of the electrocatalysts over the course of AST (protocol III), (b, c) R_Σ and C_{lim} of electrocatalysts obtained at DC bias potential of 0.425 V_{RHE}, (d) ORR mass activity (i_m) of electrocatalysts.

406

Table 3. Electrochemical characterization of electrocatalysts

Catalyst	P_t mg cm^{-2}	ECSA m^2 g^{-1}	I @ 0.9 mA/mg$_{Pt}$	I @ 0.9 mA cm^{-2}	Media	Stability protocol	ECSA loss cycle	Ref.
Pt/Nbo/CNTs	0.02	81.62	57	1.14	0.5M H_2SO_4	(I) (II) (III)	5%-5k 7.4%-30k 11.4%-10k	current study
Pt/CNTs	0.02	76.85	43	0.86	0.5M H_2SO_4	(I) (II) (III)	64.4%-5k 18.3%-30k 32.2%-10k	current study
Pt/C	0.02	73.66	28.5	0.57	0.5M H_2SO_4	(I) (II) (III)	73.2%-5k 47.6%-30k 78.5%-10k	current study
Pt-Ta_2O_5/CNT	0.02	78.4		0.29	0.1M $HClO_4$	(II)	4.1%-10k	[79]
Pt/CNT	0.02	67.1		0.15	0.1M $HClO_4$	(II)	42%-10k	[79]
Pt/C	0.02	61.9		0.11	0.1M $HClO_4$	(II)	49.9%-10k	[79]
Pt/TiO_2/G-ATV	0.101	40.4	4.95	0.5	0.5M H_2SO_4	(I)	77%-4k	[4]
Pt/TiO_2-CN_x	-	75	<10	-	0.5M H_2SO_4	(II)	3%-1k	[83]
Pt/NbO_2/C	0.005	68	-	1	0.1M $HClO_4$	(II)	45%-30k	[1]
Pt/PdCu/C	0.02	83.2	-	2.5	0.1M $HClO_4$	(I)	30%-0.5k	[84]
Pt/IrO_2 Nb_2O_5-rGO	0.057	69.5	8.5	0.48	0.5M H_2SO_4	(I)	23.8%-2k	[85]
Pt/TiO_x/CNT	0.0136	44.13	10.7	0.3	0.1M $HClO_4$	(I)	<1%-4k	[7]

407
408
409

3.5 Performance of Pt/NbO/CNTs on PEMFC

Figure 10a shows the polarization and power density curves achieved using the Pt/NbO/CNTs electrocatalyst at the cathode, running the PEMFC at different temperatures. The performance at 80 °C was compared to that of a MEA with Pt/C electrodes at both sides (**Fig. 10b**); the Pt/NbO/CNTs reached a maximum of power density of 772 mW cm^{-2}, respect to 680 mW cm^{-2} of the Pt/C. These results indicate an enhanced electroactivity of Pt supported on hybrid NbO/CNTs support towards ORR. The high power density of Pt/NbO/CNTs can be attributed to the good charge transfer between Pt and NbO support, which favors the oxygen reduction kinetics [17,86]. In fact, supporting materials can have a great influence on the activity of electrocatalysts by promoting the diffusion of reactants and products [9,35,87,88].

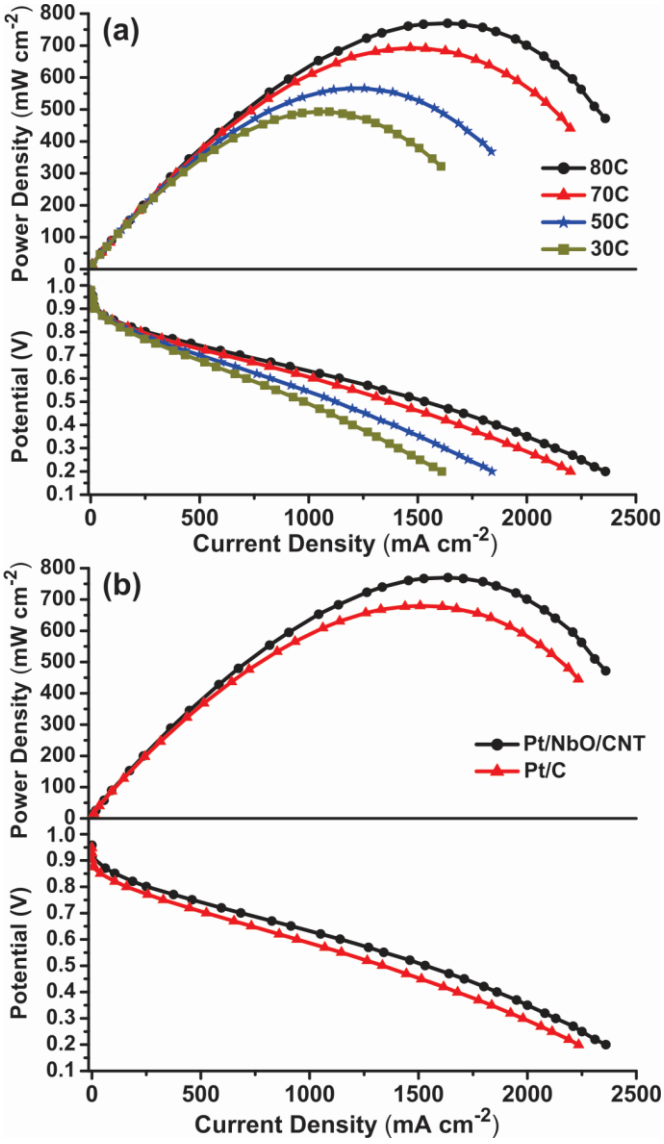

Figure 10. (a) PEMFC performance of the Pt/NbO/CNTs, polarization and power density curves as a function of the temperature, (b) Comparison of the fuel cell performance obtained using the Pt/NbO/CNTs and Pt/C electrodes. Measurements were made in a 5 cm^2 single cell PEMFC at 80 °C, using a Pt loading of 0.15 mg cm^{-2}. H_2 flow rate of 120 nml min^{-1} 100% RH 1 bar bp; O_2 flow rate 200 nml min^{-1} 100% RH 1 bar bp, and membrane of NRE212.

The short-term stability on the Pt/NbO/CNTs electrode was assessed by maintained in operation at the maximum current density at 80 °C for 96 consecutive hours and Polarization curves were collected every 24 hours. **Figure 11** demonstrate the excellent stability of Pt/NbO/CNTs electrode, which lost only 4% of its maximum power, from 770 to 740 mW cm^{-2}, confirming the high stability of Pt/NbO/CNTs catalyst as already demonstrated with AST under both load cycling and Startup/Shutdown. Considering the DoE guidelines of target MEAs able to reach the equivalent of 5 mW μg_{Pt}^{-1} as mass specific power density (or a Pt usage equivalent to 200 mg_{Pt} kW^{-1}) [89,90], with the mass of Pt accounting for both anode and cathode loading, the Pt/NbO/CNTs electrode achieved a mass specific power density of almost 2.6 mW μg_{Pt}^{-1} (390 mg_{Pt} kW^{-1}). Considering also the high stability demonstrated in almost 100 hours of continuous operation, the Pt/NbO/CNTs catalyst can be considered as a promising low-Pt catalyst alternative to Pt/C for PEMFCs.

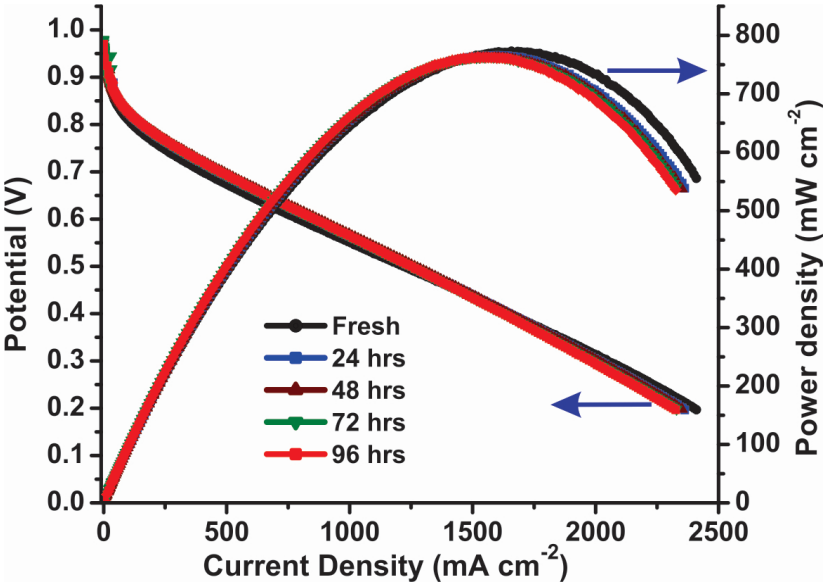

Figure 11. *in-situ* Short-term stability of Pt/NbO/CNTs. Measurements were made in a 5 cm^2 single cell PEMFC at 80 °C using a Pt loading of 0.15 mg cm^{-2}. H_2 flow rate of 120 nml min^{-1} 100% RH 1 bar bp; O_2 flow rate 200 nml min^{-1} 100% RH 1 bar bp, and membrane of NRE212.

Conclusions

This study demonstrated the NbO as an excellent metal oxide support, in combination with multi-walled carbon nanotubes (CNTs), to enhance the electrocatalytic activity of Pt towards the oxygen reduction reaction. The highly electroactive and stable electrocatalyst, synthesized by depositing Pt over a NbO/CNTs hybrid support, was used to fabricate low Pt loading MEA for PEMFC. The developed Pt/NbO/CNTs electrocatalyst showed high ORR activity comparable to Pt/CNTs and commercial Pt/C. Also, the Pt/NbO/CNTs exhibited excellent stability under both load cycling and Startup/Shutdown AST protocols. The Pt/NbO/CNTs electrode achieved to maximum power density of 770 mW cm^{-2} under fuel cell application, with only negligible decline in electroactivity (loss of power of only 4% after 96 consecutive hours of operation at 80 °C). The NbO support, in combination with CNTs, may not only improve corrosion resistance of carbon support, also promote catalytic activity and durability of Pt electrocatalyst through strong metal-support interactions. NbO demonstrated as a promising support for Pt electrocatalyst, with the

ability to mitigate one of the major problems involving carbon corrosion in acidic media. Moreover, the good performance on PEMFC obtained with a low Pt loading on the MEA makes the Pt/NbO/CNTs an excellent electro-active and stable catalyst to boosting applications of PEMFC on the market.

Acknowledgements

The authors acknowledge support from the Natural Sciences and Engineering Research Council (NSERC) of Canada through the Discovery Grants program (RGPIN- 003652-2015) and University of Ontario Institute of Technology (UOIT). The authors acknowledge equipment support from the Canada Foundation for Innovation. The authors thank Advanced Energy Lab (Environmental Park, Torino. Italy) for the use of PEMFC station.

References

[1] K. Sasaki, L. Zhang, R.R. Adzic, Niobium oxide-supported platinum ultra-low amount electrocatalysts for oxygen reduction, Phys. Chem. Chem. Phys. 10 (2008) 159–167. https://doi.org/10.1039/B709893F.

[2] H.A. Gasteiger, S.S. Kocha, B. Sompalli, F.T. Wagner, Activity benchmarks and requirements for Pt, Pt-alloy, and non-Pt oxygen reduction catalysts for PEMFCs, Appl. Catal. B Environ. 56 (2005) 9–35. https://doi.org/10.1016/j.apcatb.2004.06.021.

[3] S. Siracusano, A. Stassi, E. Modica, V. Baglio, A.S. Aricò, Preparation and characterisation of Ti oxide based catalyst supports for low temperature fuel cells, Int. J. Hydrogen Energy. 38 (2013) 11600–11608. https://doi.org/10.1016/j.ijhydene.2013.04.161.

[4] C. Odetola, L. Trevani, E.B. Easton, Enhanced activity and stability of Pt/TiO2/carbon fuel cell electrocatalyst prepared using a glucose modifier, J. Power Sources. 294 (2015) 254–263. https://doi.org/10.1016/j.jpowsour.2015.06.066.

[5] S. Specchia, C. Francia, P. Spinelli, Polymer Electrolyte Membrane Fuel Cells, in: Electrochem. Technol. Energy Storage Convers., 2011: pp. 601–670. https://doi.org/10.1002/9783527639496.ch13.

[6] C. He, S. Desai, G. Brown, S. Bollepalli, PEM Fuel Cell Catalysts: Cost, Performance, and Durability, Electrochem. Soc. Interface. (2005) 41–44.

[7] R. Alipour Moghadam Esfahani, A.H.A. Monteverde Videla, S. Vankova, S. Specchia, Stable and methanol tolerant Pt/TiOx-C electrocatalysts for the oxygen reduction reaction, Int. J. Hydrogen Energy. 40 (2015) 14529–14539. https://doi.org/10.1016/j.ijhydene.2015.05.131.

[8] C. Odetola, L.N. Trevani, E.B. Easton, Photo enhanced methanol electrooxidation: Further insights into Pt and TiO2 nanoparticle contributions, Appl. Catal. B Environ. 210 (2017) 263–275. https://doi.org/10.1016/j.apcatb.2017.03.027.

[9] Z. Zhang, J. Liu, J. Gu, L. Su, L. Cheng, An overview of metal oxide materials as electrocatalysts and supports for polymer electrolyte fuel cells, Energy Environ. Sci. 7 (2014) 2535–2558. https://doi.org/10.1039/C3EE43886D.

[10] D. Sebastián, V. Baglio, S. Sun, A.C. Tavares, A.S. Aricò, Facile synthesis of Zr- and Ta-based catalysts for the oxygen reduction reaction, Chinese J. Catal. 36 (2015) 484–489. https://doi.org/10.1016/S1872-

2067(14)60253-9.
[11] Y. Xiao, G. Zhan, Z. Fu, Z. Pan, C. Xiao, S. Wu, C. Chen, G. Hu, Z. Wei, Robust non-carbon titanium nitride nanotubes supported Pt catalyst with enhanced catalytic activity and durability for methanol oxidation reaction, Electrochim. Acta. 141 (2014) 279–285. https://doi.org/10.1016/j.electacta.2014.07.070.
[12] P. Justin, P. Hari Krishna Charan, G. Ranga Rao, High performance Pt–Nb2O5/C electrocatalysts for methanol electrooxidation in acidic media, Appl. Catal. B Environ. 100 (2010) 510–515. https://doi.org/10.1016/j.apcatb.2010.09.001.
[13] A. Kostuch, J. Gryboś, P. Indyka, L. Osmieri, S. Specchia, Z. Sojka, K. Kruczała, Morphology and dispersion of nanostructured manganese-cobalt spinel on various carbon supports: The effect on the oxygen reduction reaction in alkaline media, Catal. Sci. Technol. 8 (2018) 642–655. https://doi.org/10.1039/c7cy02228j.
[14] R. Alipour Moghadam Esfahani, H.M. Fruehwald, F. Afsahi, E.B. Easton, Enhancing fuel cell catalyst layer stability using a dual-function sulfonated silica-based ionomer, Appl. Catal. B Environ. 232 (2018) 314–321. https://doi.org/10.1016/j.apcatb.2018.03.080.
[15] M. Tian, G. Wu, A. Chen, Unique Electrochemical Catalytic Behavior of Pt Nanoparticles Deposited on TiO2 Nanotubes, ACS Catal. 2 (2012) 425–432. https://doi.org/10.1021/cs200691a.
[16] J. Zhang, M.B. Vukmirovic, K. Sasaki, A.U. Nilekar, M. Mavrikakis, R.R. Adzic, Mixed-metal Pt monolayer electrocatalysts for enhanced oxygen reduction kinetics, J. Am. Chem. Soc. 127 (2005) 12480–12481. https://doi.org/10.1021/ja053695i.
[17] S.-Y. Huang, P. Ganesan, B.N. Popov, Electrocatalytic Activity and Stability of Titania-Supported Platinum–Palladium Electrocatalysts for Polymer Electrolyte Membrane Fuel Cell, ACS Catal. 2 (2012) 825–831. https://doi.org/10.1021/cs300088n.
[18] P. Marques, N.F.P. Ribeiro, M. Schmal, D.A.G. Aranda, M.M.V.M. Souza, Selective CO oxidation in the presence of H2 over Pt and Pt-Sn catalysts supported on niobia, J. Power Sources. 158 (2006) 504–508. https://doi.org/10.1016/j.jpowsour.2005.09.035.
[19] V.R. Stamenkovic, B. Fowler, B.S. Mun, G. Wang, P.N. Ross, C.A. Lucas, N.M. Markovic, Improved Oxygen Reduction Activity on Pt3Ni(111) via Increased Surface Site Availability, Science (80-.). 315 (2007) 493–497. https://doi.org/10.1126/science.1135941.
[20] C. Dupont, Y. Jugnet, D. Loffreda, Theoretical evidence of PtSn alloy efficiency for CO oxidation, J. Am. Chem. Soc. 128 (2006) 9129–9136. https://doi.org/10.1021/ja061303h.
[21] S.L. Knupp, M.B. Vukmirovic, P. Haldar, J.A. Herron, M. Mavrikakis, R.R. Adzic, Platinum Monolayer Electrocatalysts for O2 Reduction: Pt Monolayer on Carbon-Supported PdIr Nanoparticles, Electrocatalysis. 1 (2010) 213–223. https://doi.org/10.1007/s12678-010-0028-8.
[22] F.D. Kong, G.P. Yin, C.Y. Du, S. Zhang, Y.T. Qu, L. Du, Z.Q. Xu, A.X. Ling, 3D-niobium oxide supported platinum as an effective and durable oxygen reduction catalyst, Catal. Commun. 68 (2015) 67–72. https://doi.org/10.1016/j.catcom.2015.05.003.
[23] K. Senevirathne, R. Hui, S. Campbell, S. Ye, J. Zhang, Electrocatalytic activity and durability of Pt/NbO2

519 and Pt/Ti4O7 nanofibers for PEM fuel cell oxygen reduction reaction, Electrochim. Acta. 59 (2012) 538–
520 547. https://doi.org/10.1016/j.electacta.2011.11.005.
521 [24] L. Zhang, L. Wang, C.M.B. Holt, T. Navessin, K. Malek, M.H. Eikerling, D. Mitlin, Oxygen reduction
522 reaction activity and electrochemical stability of thin-film bilayer systems of platinum on niobium oxide, J.
523 Phys. Chem. C. 114 (2010) 16463–16474. https://doi.org/10.1021/jp104306j.
524 [25] Q. Du, J. Wu, H. Yang, Pt@Nb-TiO2 catalyst membranes fabricated by electrospinning and atomic layer
525 deposition, ACS Catal. 4 (2014) 144–151. https://doi.org/10.1021/cs400944p.
526 [26] H.J. Chun, D.B. Kim, D.H. Lim, W.D. Lee, H.I. Lee, A synthesis of CO-tolerant Nb2O5-promoted Pt/C
527 catalyst for direct methanol fuel cell; Its physical and electrochemical characterization, Renew. Energy. 35
528 (2010) 6399–6408. https://doi.org/10.1016/j.ijhydene.2010.03.061.
529 [27] K. Sasaki, R.R. Adzic, Monolayer-Level Ru- and NbO2-Supported Platinum Electrocatalysts for Methanol
530 Oxidation, J. Electrochem. Soc. 155 (2008) B180. https://doi.org/10.1149/1.2816238.
531 [28] C. Nico, T. Monteiro, M.P.F. Graça, Niobium oxides and niobates physical properties: Review and
532 prospects, Prog. Mater. Sci. 80 (2016) 1–37. https://doi.org/10.1016/j.pmatsci.2016.02.001.
533 [29] R. Alipour Moghadam Esfahani, S.K. Vankova, A.H.A. Monteverde Videla, S. Specchia, Innovative
534 carbon-free low content Pt catalyst supported on Mo-doped titanium suboxide (Ti 3 O 5 -Mo) for stable
535 and durable oxygen reduction reaction, Appl. Catal. B Environ. 201 (2017) 419–429.
536 https://doi.org/10.1016/j.apcatb.2016.08.041.
537 [30] J. Zeng, C. Francia, M.A. Dumitrescu, A.H.A. Monteverde Videla, V.S. Ijeri, S. Specchia, P. Spinelli,
538 Electrochemical performance of Pt-based catalysts supported on different ordered mesoporous carbons
539 (Pt/OMCs) for oxygen reduction reaction, Ind. Eng. Chem. Res. 51 (2012) 7500–7509.
540 https://doi.org/10.1021/ie2016619.
541 [31] Y. Garsany, J. Ge, J. St-Pierre, R. Rocheleau, K.E. Swider-Lyons, Analytical Procedure for Accurate
542 Comparison of Rotating Disk Electrode Results for the Oxygen Reduction Activity of Pt/C, J. Electrochem.
543 Soc. 161 (2014) F628–F640. https://doi.org/10.1149/2.036405jes.
544 [32] R. Cuccaro, M. Lucariello, A. Battaglia, A. Graizzaro, Research of a HySyLab internal standard procedure
545 for single PEMFC, Int. J. Hydrogen Energy. 33 (2008) 3159–3166.
546 https://doi.org/10.1016/j.ijhydene.2008.04.016.
547 [33] G. Sun, X. Li, Y. Qu, X. Wang, H. Yan, Y. Zhang, Preparation and characterization of graphite nanosheets
548 from detonation technique, Mater. Lett. 62 (2008) 703–706. https://doi.org/10.1016/j.matlet.2007.06.035.
549 [34] L. Osmieri, A.H.A. Monteverde Videla, S. Specchia, Activity of Co-N multi walled carbon nanotubes
550 electrocatalysts for oxygen reduction reaction in acid conditions, J. Power Sources. 278 (2015) 296–307.
551 https://doi.org/10.1016/j.jpowsour.2014.12.080.
552 [35] Y. Zhang, J. Zang, L. Dong, X. Cheng, Y. Zhao, Y. Wang, A Ti-coated nano-SiC supported platinum
553 electrocatalyst for improved activity and durability in direct methanol fuel cells, J. Mater. Chem. A. 2
554 (2014) 10146. https://doi.org/10.1039/c4ta00618f.
555 [36] D. Li, C. Wang, D.S. Strmcnik, D. V. Tripkovic, X. Sun, Y. Kang, M. Chi, J.D. Snyder, D. van der Vliet,
556 Y. Tsai, V.R. Stamenkovic, S. Sun, N.M. Markovic, Functional links between Pt single crystal morphology

and nanoparticles with different size and shape: the oxygen reduction reaction case, Energy Environ. Sci. 7 (2014) 4061–4069. https://doi.org/10.1039/C4EE01564A.

[37] S. Gallego, Surface-layered ordered alloy (Pt/Pt3 Mn) on Pt (111), Phys. Rev. B. 56 (1997) 139–142.

[38] J. Wu, J. Zhang, Z. Peng, S. Yang, F.T. Wagner, H. Yang, Truncated octahedral Pt3Ni oxygen reduction reaction electrocatalysts, J. Am. Chem. Soc. 132 (2010) 4984–4985. https://doi.org/10.1021/ja100571h.

[39] Y.J. Wang, N. Zhao, B. Fang, H. Li, X.T. Bi, H. Wang, Carbon-Supported Pt-Based Alloy Electrocatalysts for the Oxygen Reduction Reaction in Polymer Electrolyte Membrane Fuel Cells: Particle Size, Shape, and Composition Manipulation and Their Impact to Activity, Chem. Rev. 115 (2015) 3433–3467. https://doi.org/10.1021/cr500519c.

[40] J. He, Y. Hu, Z. Wang, W. Lu, S. Yang, G. Wu, Y. Wang, S. Wang, H. Gu, J. Wang, Hydrothermal growth and optical properties of Nb2O5 nanorod arrays, J. Mater. Chem. C. 2 (2014) 8185–8190. https://doi.org/10.1039/c4tc01581a.

[41] J. Xue, R. Wang, Z. Zhang, S. Qiu, Facile preparation of C, N co-modified Nb2O5 nanoneedles with enhanced visible light photocatalytic activity, Dalt. Trans. 45 (2016) 16519–16525. https://doi.org/10.1039/c6dt03548e.

[42] J.K. Dash, L. Chen, M.R. Topka, P.H. Dinolfo, L.H. Zhang, K. Kisslinger, T.M. Lu, G.C. Wang, A simple growth method for Nb2O5 films and their optical properties, RSC Adv. 5 (2015) 36129–36139. https://doi.org/10.1039/c5ra05074j.

[43] A. Gupta, M. Mittal, M.K. Singh, S.L. Suib, O.P. Pandey, Low temperature synthesis of NbC/C nano-composites as visible light photoactive catalyst, Sci. Rep. 8 (2018) 1–17. https://doi.org/10.1038/s41598-018-31989-z.

[44] A.S. Trifonov, A. V. Lubenchenko, V.I. Polkin, A.B. Pavolotsky, S. V. Ketov, D. V. Louzguine-Luzgin, Difference in charge transport properties of Ni-Nb thin films with native and artificial oxide, J. Appl. Phys. 117 (2015). https://doi.org/10.1063/1.4915935.

[45] X. Huang, Z. Zhao, L. Cao, Y. Chen, E. Zhu, Z. Lin, M. Li, A. Yan, A. Zettl, Y.M. Wang, X. Duan, T. Mueller, Y. Huang, High-performance transition metal-doped Pt3Ni octahedra for oxygen reduction reaction, Science (80-.). 348 (2015) 1230–1234. https://doi.org/10.1126/science.aaa8765.

[46] R. Alipour Moghadam Esfahani, R.B. Moghaddam, I.I. Ebralidze, E.B. Easton, A hydrothermal approach to access active and durable sulfonated silica-ceramic carbon electrodes for PEM fuel cell applications, Appl. Catal. B Environ. 239 (2018) 125–132. https://doi.org/10.1016/j.apcatb.2018.07.077.

[47] G. Long, X. Li, K. Wan, Z. Liang, J. Piao, P. Tsiakaras, Pt/CN-doped electrocatalysts: Superior electrocatalytic activity for methanol oxidation reaction and mechanistic insight into interfacial enhancement, Appl. Catal. B Environ. 203 (2017) 541–548. https://doi.org/10.1016/j.apcatb.2016.10.055.

[48] R. Alipour Moghadam Esfahani, I.I. Ebralidze, S. Specchia, E.B. Easton, A fuel cell catalyst support based on doped titanium suboxides with enhanced conductivity, durability and fuel cell performance, J. Mater. Chem. A. 6 (2018) 14805–14815. https://doi.org/10.1039/c8ta02470g.

[49] R. Alipour Moghadam Esfahani, Luis Miguel Rivera Gavidia c, G. García, E. Pastor, S. Specchia, Highly active platinum supported on Mo-doped titanium nanotubes suboxide (Pt/TNTS-Mo) electrocatalyst for

oxygen reduction reaction in PEMFC, Renew. Energy. 120 (2018) 209–219. https://doi.org/https://doi.org/10.1016/j.renene.2017.12.077.

[50] F. Li, H.M. Cheng, Y.T. Xing, P.H. Tan, G. Su, Purification of single-walled carbon nanotubes synthesized by the catalytic decomposition of hydrocarbons, Carbon N. Y. 38 (2000) 2041–2045. https://doi.org/10.1016/S0008-6223(00)00061-0.

[51] V. Datsyuk, M. Kalyva, K. Papagelis, J. Parthenios, D. Tasis, A. Siokou, I. Kallitsis, C. Galiotis, Chemical oxidation of multiwalled carbon nanotubes, Carbon N. Y. 46 (2008) 833–840. https://doi.org/10.1016/j.carbon.2008.02.012.

[52] L. Krishnia, V. Kumar, R. Kumari, P. Garg, B.S. Yadav, A. Rath, A. Ghosh, R.K. Sinha, M.K. Singh, P.K. Tyagi, Exclusive Endothermic Oxidation of Fe₃C-Filled Multi-Walled Carbon Nanotubes, Adv. Sci. Eng. Med. 8 (2016) 460–467. https://doi.org/10.1166/asem.2016.1876.

[53] D. Luxembourg, G. Flamant, D. Laplaze, Solar synthesis of single-walled carbon nanotubes at medium scale, Carbon N. Y. 43 (2005) 2302–2310. https://doi.org/10.1016/j.carbon.2005.04.010.

[54] H.M. Fruehwald, I.I. Ebralidze, O. V. Zenkina, E.B. Easton, Fe−N 3 /C Active Catalytic Sites for the Oxygen Reduction Reaction Prepared with Molecular-Level Geometry Control through the Covalent Immobilization of an Iron−Terpyridine Motif onto Carbon, ChemElectroChem. 6 (2019) 1350–1358. https://doi.org/10.1002/celc.201801842.

[55] H.A. Gasteiger, J.E. Panels, S.G. Yan, Dependence of PEM fuel cell performance on catalyst loading, J. Power Sources. 127 (2004) 162–171. https://doi.org/10.1016/j.jpowsour.2003.09.013.

[56] R. Alipour Moghadam Esfahani, H.M. Fruehwald, N.O. Laschuk, M.T. Sullivan, J.G. Egan, I.I. Ebralidze, O. V Zenkina, E.B. Easton, A highly durable N-enriched titanium nanotube suboxide fuel cell catalyst support, Appl. Catal. B Environ. 263 (2020) 118272. https://doi.org/10.1016/j.apcatb.2019.118272.

[57] H.R. Colón-Mercado, B.N. Popov, Stability of platinum based alloy cathode catalysts in PEM fuel cells, J. Power Sources. 155 (2006) 253–263. https://doi.org/10.1016/j.jpowsour.2005.05.011.

[58] J. Zeng, C. Francia, C. Gerbaldi, M.A. Dumitrescu, S. Specchia, P. Spinelli, Smart synthesis of hollow core mesoporous shell carbons (HCMSC) as effective catalyst supports for methanol oxidation and oxygen reduction reactions, J. Solid State Electrochem. 16 (2012) 3087–3096. https://doi.org/10.1007/s10008-012-1750-3.

[59] E. Passalacqua, F. Lufrano, G. Squadrito, A. Patti, L. Giorgi, Nafion content in the catalyst layer of polymer electrolyte fuel cells: Effects on structure and performance, Electrochim. Acta. 46 (2001) 799–805. https://doi.org/10.1016/S0013-4686(00)00679-4.

[60] S.H. Joo, K. Kwon, D.J. You, C. Pak, H. Chang, J.M. Kim, Preparation of high loading Pt nanoparticles on ordered mesoporous carbon with a controlled Pt size and its effects on oxygen reduction and methanol oxidation reactions, Electrochim. Acta. 54 (2009) 5746–5753. https://doi.org/10.1016/j.electacta.2009.05.022.

[61] G.-F. Wei, Z.-P. Liu, Towards active and stable oxygen reduction cathodes: a density functional theory survey on Pt2M skin alloys, Energy Environ. Sci. 4 (2011) 1268. https://doi.org/10.1039/c0ee00762e.

[62] K. Huang, K. Sasaki, R.R. Adzic, Y. Xing, Increasing Pt oxygen reduction reaction activity and durability

with a carbon-doped TiO2 nanocoating catalyst support, J. Mater. Chem. 22 (2012) 16824. https://doi.org/10.1039/c2jm32234j.

[63] J. Zhang, M.B. Vukmirovic, Y. Xu, M. Mavrikakis, R.R. Adzic, Controlling the Catalytic Activity of Platinum-Monolayer Electrocatalysts for Oxygen Reduction with Different Substrates, Angew. Chemie Int. Ed. 44 (2005) 2132–2135. https://doi.org/10.1002/anie.200462335.

[64] V.T.T. Ho, C.J. Pan, J. Rick, W.N. Su, B.J. Hwang, Nanostructured Ti0.7Mo0.3O2 support enhances electron transfer to Pt: High-performance catalyst for oxygen reduction reaction, J. Am. Chem. Soc. 133 (2011) 11716–11724. https://doi.org/10.1021/ja2039562.

[65] J.X. Wang, F.A. Uribe, T.E. Springer, J. Zhang, R.R. Adzic, Intrinsic kinetic equation for oxygen reduction reaction in acidic media: the double Tafel slope and fuel cell applications, Faraday Discuss. 140 (2008) 347–362. https://doi.org/10.1039/B814058H.

[66] A. Holewinski, S. Linic, Elementary mechanisms in electrocatalysis: Revisiting the ORR tafel slope, J. Electrochem. Soc. 159 (2012) 864–870. https://doi.org/10.1149/2.022211jes.

[67] R. Alipour Moghadam Esfahani, R.B. Moghaddam, E.B. Easton, High performance Pt/Ti3O5Mo0.2Si0.4 electrocatalyst with outstanding methanol oxidation activity, Catal. Sci. Technol. 9 (2019) 4118–4124. https://doi.org/10.1039/c9cy00704k.

[68] M.A. Scibioh, S.K. Kim, E.A. Cho, T.H. Lim, S.A. Hong, H.Y. Ha, Pt-CeO2/C anode catalyst for direct methanol fuel cells, Appl. Catal. B Environ. 84 (2008) 773–782. https://doi.org/10.1016/j.apcatb.2008.06.017.

[69] B. Abida, L. Chirchi, S. Baranton, T.W. Napporn, H. Kochkar, J.-M. Léger, A. Ghorbel, Preparation and characterization of Pt/TiO2 nanotubes catalyst for methanol electro-oxidation, Appl. Catal. B Environ. 106 (2011) 609–615. https://doi.org/10.1016/j.apcatb.2011.06.022.

[70] J. Wang, J. Xi, Y. Bai, Y. Shen, J. Sun, L. Chen, W. Zhu, X. Qiu, Structural designing of Pt-CeO2/CNTs for methanol electro-oxidation, J. Power Sources. 164 (2007) 555–560. https://doi.org/10.1016/j.jpowsour.2006.11.041.

[71] J.I. Eastcott, J.A. Powell, A.J. Vreugdenhil, E.B. Easton, Electrochemical and Morphological Studies of Ceramic Carbon Electrodes for Fuel Cell Systems, ECS Trans. 41 (2011) 853–864. https://doi.org/Doi 10.1149/1.3635619.

[72] E.B. Easton, P.G. Pickup, An electrochemical impedance spectroscopy study of fuel cell electrodes, Electrochim. Acta. 50 (2005) 2469–2474. https://doi.org/10.1016/j.electacta.2004.10.074.

[73] F.S. Saleh, E.B. Easton, Diagnosing Degradation within PEM Fuel Cell Catalyst Layers Using Electrochemical Impedance Spectroscopy, J. Electrochem. Soc. 159 (2012) B546–B553. https://doi.org/10.1149/2.098205jes.

[74] Y. Shao, G. Yin, Y. Gao, Understanding and approaches for the durability issues of Pt-based catalysts for PEM fuel cell, J. Power Sources. 171 (2007) 558–566. https://doi.org/10.1016/j.jpowsour.2007.07.004.

[75] F.S. Saleh, E.B. Easton, Assessment of the ethanol oxidation activity and durability of Pt catalysts with or without a carbon support using Electrochemical Impedance Spectroscopy, J. Power Sources. 246 (2014) 392–401. https://doi.org/10.1016/j.jpowsour.2013.07.109.

[76] J. Parrondo, T. Han, E. Niangar, C. Wang, N. Dale, K. Adjemian, V. Ramani, Platinum supported on titanium-ruthenium oxide is a remarkably stable electrocatayst for hydrogen fuel cell vehicles, Proc. Natl. Acad. Sci. U. S. A. 111 (2014) 45–50. https://doi.org/10.1073/pnas.1319663111.

[77] Z. Song, B. Wang, N. Cheng, L. Yang, D. Banham, R. Li, S. Ye, X. Sun, Atomic layer deposited tantalum oxide to anchor Pt/C for a highly stable catalyst in PEMFCs, J. Mater. Chem. A. 5 (2017) 9760–9767. https://doi.org/10.1039/c7ta01926b.

[78] H. Schmies, A. Bergmann, J. Drnec, G. Wang, D. Teschner, S. Kühl, D.J.S. Sandbeck, S. Cherevko, M. Gocyla, M. Shviro, M. Heggen, V. Ramani, R.E. Dunin-Borkowski, K.J.J. Mayrhofer, P. Strasser, Unravelling Degradation Pathways of Oxide-Supported Pt Fuel Cell Nanocatalysts under In Situ Operating Conditions, Adv. Energy Mater. 8 (2018) 1–13. https://doi.org/10.1002/aenm.201701663.

[79] W. Gao, Z. Zhang, M. Dou, F. Wang, Highly Dispersed and Crystalline Ta2O5 Anchored Pt Electrocatalyst with Improved Activity and Durability Toward Oxygen Reduction: Promotion by Atomic-Scale Pt-Ta2O5 Interactions, ACS Catal. 9 (2019) 3278–3288. https://doi.org/10.1021/acscatal.8b04505.

[80] Q. Wang, N. Dai, J. Zheng, J.P. Zheng, Preparation and catalytic performance of Pt supported on Nafion® functionalized carbon nanotubes, J. Electroanal. Chem. 854 (2019) 113508. https://doi.org/10.1016/j.jelechem.2019.113508.

[81] L. Li, Y. Xing, Pt-Ru nanoparticles supported on carbon nanotubes as methanol fuel cell catalysts, AIChE Annu. Meet. Conf. Proc. (2006) 2803–2808.

[82] R. Alipour Moghadam Esfahani, E.B. Easton, Exceptionally durable Pt/TOMS catalysts for fuel cells Reza, Appl. Catal. B Environ. (2020). https://doi.org/10.1016/j.apcatb.2020.118743.

[83] J. Tang, H.M. Meng, TiO 2 -modified CN x nanowires as a Pt electrocatalyst support with high activity and durability for the oxygen reduction reaction, Phys. Chem. Chem. Phys. 18 (2016) 1500–1506. https://doi.org/10.1039/c5cp06115f.

[84] T. Cochell, A. Manthiram, Pt@Pd xCu y/C core-shell electrocatalysts for oxygen reduction reaction in fuel cells, Langmuir. 28 (2012) 1579–1587. https://doi.org/10.1021/la202610z.

[85] F.D. Kong, L.J. Yang, J. Liu, A.X. Ling, M.J. Shi, M. Lv, Z.Q. Xu, Y.L. Niu, H.Y. Wang, Fabrication of Pt/IrO2Nb2O5–rGO Electrocatalyst by Support Improvement for Oxygen Reduction Reaction, Catal. Letters. 149 (2019) 3041–3047. https://doi.org/10.1007/s10562-019-02875-8.

[86] V. Celorrio, J. Flórez-Montaño, R. Moliner, E. Pastor, M.J. Lázaro, Fuel cell performance of Pt electrocatalysts supported on carbon nanocoils, Int. J. Hydrogen Energy. 39 (2014) 5371–5377. https://doi.org/10.1016/j.ijhydene.2013.12.198.

[87] J. Rodriguez, Physical and chemical properties of bimetallic surfaces, Surf. Sci. Rep. 24 (1996) 223–287. https://doi.org/10.1016/0167-5729(96)00004-0.

[88] M.K. Debe, A.K. Schmoeckel, G.D. Vernstrom, R. Atanasoski, High voltage stability of nanostructured thin film catalysts for PEM fuel cells, J. Power Sources. 161 (2006) 1002–1011. https://doi.org/10.1016/j.jpowsour.2006.05.033.

[89] S.S. Kocha, J.W. Zack, K. Shinozaki, S. Pylypenko, V. Stamenkovic, Y. Kang, D. Li, D. Myers, N. Kariuki, T. Nowicki, D. Manager David Peterson, Best Practices and Benchmark Activities for ORR

709 Measurements by the Rotating Disk Electrode Technique - DOE Hydrogen and Fuel Cells Program FY
710 2014 Annual Progress Report, (2013).
711 [90] A. Brouzgou, S.Q. Song, P. Tsiakaras, Low and non-platinum electrocatalysts for PEMFCs: Current status,
712 challenges and prospects, Appl. Catal. B Environ. 127 (2012) 371–388.
713 https://doi.org/10.1016/j.apcatb.2012.08.031.
714